Review Article

Yousef Rasmi, Kevser K. Kırboğa, Johra Khan, Ena Gupta, Fadia Mostafa, Murali M. Yallapu, and Fernanda Pilaquinga*

Gold nanoparticle-based strategies against SARS-CoV-2: A review

https://doi.org/10.1515/rams-2023-0105
received February 24, 2023; accepted July 21, 2023

Abstract: The COVID-19 pandemic caused by severe acute respiratory syndrome coronavirus 2 has been an immense threat to global public health and has also had a negative socioeconomic impact worldwide. However, although the pandemic is now under control, it has demonstrated that society is unprepared to use analysis methods that are applicable to various types of viruses nor apply new therapies to prevent infections, considering the extensive time needed for vaccine development. The use of nanomaterial-based diagnostics and therapeutics can provide essential strategies for both virus detection and treatment. Gold nanoparticles (AuNPs) are the nanomaterials most commonly used to enhance virus detection because of their bioconjugation, high plasmon resonance, and excellent electrical, optical, and catalytic properties. The present review outlines the recent advances reported in the literature regarding using AuNPs for their antiviral activities with respiratory viruses, analysis techniques such as AuNP-assisted polymerase chain reaction, biosensors (electrochemical, piezoelectric, and optical), lateral flow analysis, nucleic acid assays, and gene and vaccine therapy. Finally, as a potential antiviral treatment, this review provides *in vitro* and *in vivo* toxicity results of AuNPs for respiratory viruses, as well as those related to their toxicity in humans, to evaluate their use as a future antiviral treatment.

Keywords: gold nanoparticles, detection techniques, coronavirus SARS-CoV-2, COVID-19, toxicity, *in vivo*, *in vitro*

*** Corresponding author: Fernanda Pilaquinga**, School of Chemical Sciences, Pontificia Universidad Católica del Ecuador, Quito, Ecuador, e-mail: mfpilaquingaf@puce.edu.ec
Yousef Rasmi: Cellular and Molecular Research Center, Cellular and Molecular Medicine Institute, Urmia University of Medical Sciences, Urmia, Iran; Department of Biochemistry, School of Medicine, Urmia University of Medical Sciences, Urmia, Iran, e-mail: rasmiy@umsu.ac.ir
Kevser K. Kırboğa: Bioengineering Department, Bilecik Seyh Edebali University, Bilecik, Turkey, e-mail: kubra.kirboga@bilecik.edu.tr
Johra Khan: Department of Medical Laboratory Sciences, College of Applied Medical Sciences, Majmaah University, Majmaah, Saudi Arabia, e-mail: j.khan@mu.edu.sa
Ena Gupta: Department of Home Science, University of Allahabad, Allahabad, India, e-mail: enaravish@gmail.com
Fadia Mostafa: Department of Clinical Pathology, Suez Canal University, Ismailia, Egypt, e-mail: fadiamostafa@gmail.com
Murali M. Yallapu: Department of Immunology and Microbiology, School of Medicine, University of Texas Rio Grande Valley, McAllen, Texas, United States of America, e-mail: murali.yallapu@utrgv.edu

Abbreviations

ALP	alkaline phosphatase
ALT	alanine transaminase
AST	aspartate transaminase
AuNPs	gold nanoparticle
AuNRs	gold nanorods
AuNSs	gold nanospheres
CALNN	pentapeptide: cysteine–alanine–leucine–asparagine–asparagine
CREA	creatinine
CTAB	cetyltrimethylammonium bromide
HCT	hematocrit
MEEE	2-(2-(2-mercaptoethoxy)ethoxy)ethanol
MES	2-mercaptoethanesulfonic acid
N/R	not reported
PAH	polyallylamine hydrochloride
PEG	polyethylene glycol
PEI2	polyethyleneimine
PSS	polystyrene sulphate
RBC	red blood cells
TMAT	*N*,*N*,*N*-trimethylammonium ethanethiol
WBC	white blood cells

1 Introduction

The severe acute respiratory syndrome coronavirus 2 (SARS-CoV-2) that causes COVID-19 was first detected in December 2019 in Wuhan, China [1]. SARS-CoV-2 belongs

to the Coronaviridae family, Betacoronavirus genus, and Sarbecovirus subgenus. According to the World Health Organization, from the start of the pandemic till June 2023, the virus has spread globally, causing 6.9 million deaths and 689 million infections (57% in men and 43% in women) [2]. Its spread has steadily normalized despite having a massive impact on health systems and economies [3]. Although vaccines have been developed to lessen symptoms, the virus has not been eradicated. The persistence of the coronavirus teaches us an important lesson: society is unprepared to stop a virus's rapid and vast spread [4,5]. In addition, a number of side effects and diseases have been reported by people with COVID-19. Although most infected individuals recover completely within a short period of time, some may experience lingering symptoms. COVID-19 can cause inflammation, damage to organs such as the heart and lungs, and neurological, cutaneous, or psychological problems that can have major long-term consequences [6].

SARS-CoV-2 has a spherical polyhedral shape measuring between 80 and 120 nm, and its genome consists of a single strand of ribonucleic acid (RNA). Regarding its protein structure, one of its essential proteins is the spike (S) glycoprotein, which binds to the specific receptor of its host with its characteristic crown-like shape. In humans, this receptor is angiotensin-converting enzyme 2 (ACE2), which is found in the respiratory, circulatory, and digestive systems [7,8]. The viral infection process begins when the S1 subunit of the S protein recognizes the ACE2 receptor. The S2 subunit then cleaves deep inside the cell, activating the transmembrane protease serine 2 and initiating the fusion mechanism. All of the virus's genetic material is deposited inside the cell, where it is quickly trapped, leading to the viral transcription process, and the new polyproteins and proteases move from the endoplasmic reticulum to the Golgi apparatus. New copies are then assembled and executed, which reinitiates the viral replication process [9].

Omicron, the fifth variant of SARS-CoV-2, is characterized by more than 30 mutations in the S protein, unlike its predecessor delta, which had approximately 10. Recent studies in murine models found that omicron efficiently replicates in upper airway mucosal cells, unlike its predecessor variants, which showed greater affinity for lung cells, specifically type II pneumocytes. This variant is far more contagious; however, its fatality rate is lower, especially in patients who have received at least two doses of the vaccine [10], although the vaccine's effectiveness on omicron is still being assessed. Thus, there is still no effective treatment available to prevent its spread. Once an organism is infected, drugs capable of limiting viral replication can be administered, facilitating a much faster recovery [11].

As the need to prevent virus spread and treat those infected has grown with the COVID-19 pandemic, nanotechnology has emerged as an alternative strategy [12]. Nanoparticles (NPs), which range in size from 1 to 100 nm, have been developed as innovative tools with diverse applications. In the biomedical field, NPs have been used as antiviral and antimicrobial agents and in biosensing, drug delivery, and imaging, among others [13–15]. NPs' unique properties, such as small size, adjustable surface load, and large surface-to-volume ratio, facilitate bioavailability and control of release time, encapsulation of various types of drugs, and increased solubility. Different NPs' potential use as antiviral candidates for respiratory diseases has already been demonstrated [16], and NP-based materials have been recognized as promising tools for stimulating or suppressing immune responses. In addition, NPs can be loaded with a variety of specific antigens, rendering them a highly promising alternative when compared to conventional vaccinology methods [17–19]. In addition to preserving the native antigen structure, NPs also improve antigen delivery and presentation to antigen-presenting cells. The main advantage of nanocarriers of vaccines is their nano-size: NPs can be administered *via* oral or nasal routes and subcutaneous or intramuscular injections, targeting central locations such as lymph nodes and penetrating mucosal and epithelial barriers [20–22].

Different NPs have already been used to improve the immunization efficacy of coronavirus vaccines; among them, polymeric, inorganic, self-assembled protein, and lipid NPs have intrinsic antigenic properties and can be loaded with coronavirus antigens [23]. NPs have also been used to stimulate cellular immunity through the targeting of dendritic cells [24,25]. In addition, as coronaviruses need to access cells during the infection process to replicate, some studies have examined NPs' ability to avoid transduction by impeding virus binding to cell surface receptors. Thus, designing NPs with the proper size and surface charge to interact with viruses or virus receptors on host cells is essential to stopping infections [26,27]. In addition, metallic NPs have been shown to limit viral replication *via* a cell–virus blocking mechanism. A number of Ag-, Zn-, carbon-, silica-, and Au-based NPs have shown considerable antiviral activity against the herpes simplex virus (HSV), influenza A, human immunodeficiency virus (HIV), human parainfluenza 3, and zika virus, among others. Further, a nanomaterial made of graphene has been able to detect coronavirus; mimicking a biosensor, its graphene coating with a monoclonal antibody makes it sensitive enough to detect 1 $fg{\cdot}mL^{-1}$ of SARS-CoV-2 with no previous treatment. Likewise, magnetite NPs coated with carboxyl polymers (pcMNPs) act as ORF1ab and R gene sensors in reverse transcription-polymerase chain reaction (RT-PCR)-

linked sensing, meaning pcMNPs may be a better option for quick diagnosis [28].

One of the most widely researched nanomaterials is gold nanoparticles (AuNPs). In fact, the evidence of colloidal gold usage in China dates back to 2500 BC, and more recently, Koch discovered gold cyanide's bacteriostatic antibiotic activity against the tubercle bacillus, which was first used in tuberculosis therapy in 1920 [29]. AuNPs, like the other noble metals, possess unique electrical, catalytic, and optical properties. AuNPs demonstrate an optical phenomenon known as surface plasmon resonance (SPR), an oscillation of electrons, at the specific wavelength of 510 nm; accordingly, AuNPs are recognized for their photothermal therapeutic capabilities. Because AuNPs are activated and produce vibrations in the presence of laser light, they are extremely beneficial in the targeted therapy of tumor cells. As a result, considerable efforts have been made in recent years regarding the development and application of AuNPs for the early detection, diagnosis, and treatment of cancer [30].

Due to their redox and electrical properties, AuNPs can act as sensors in electrochemical analysis or catalytic activity. Further, AuNPs have been used to improve the detection sensitivity of some bioanalytical techniques in viral detection [31], and they can conjugate with biomolecules such as peptides, proteins, nucleic acids, and antibodies [32].

AuNPs can also be used in the preparation of nanostructured particles for the transport and selective vectoring of drugs and therapeutic macromolecules, as well as in gene therapy (vehicleization of plasmids, DNA, RNA, and so on). Also interesting is the application of AuNPs in the construction of intelligent transporter systems that allow the release of the associated medicinal drug to be controlled in terms of location and time through the activation of either an internal or external biological stimulus [33].

Because of their antiviral and antibacterial properties and selective toxicity toward microbes, AuNPs have a wide range of biological uses. They have shown significant antiviral activity when functionalized with 1-decanesulfonic acid or 1-octanethiol against HSV, human papillomavirus (HPV), and respiratory syncytial virus (RSV) [34]. Further, several studies have shown that AuNPs have an antiviral effect specifically against respiratory virus types such as influenza A (H1N1 and H3N2), RSV, and rift valley fever (RVF) [35].

Considering the challenge that SARS-CoV-2 has represented for global public health and the importance of investigating it thoroughly, this review aims to provide an overview of the recent advances in the use of AuNPs as practical diagnostic and treatment tools for SARS-CoV-2 that can be used to mitigate the spread of COVID-19 and similar viral pandemics in the future. Antiviral activity against respiratory viruses; different methods of detection including PCR, biosensors (electrochemical, piezoelectric, and optical), lateral flow analysis (LFA), and nucleic acid assays; vaccine development; gene therapy; and toxicity of AuNPs are discussed (Figure 1).

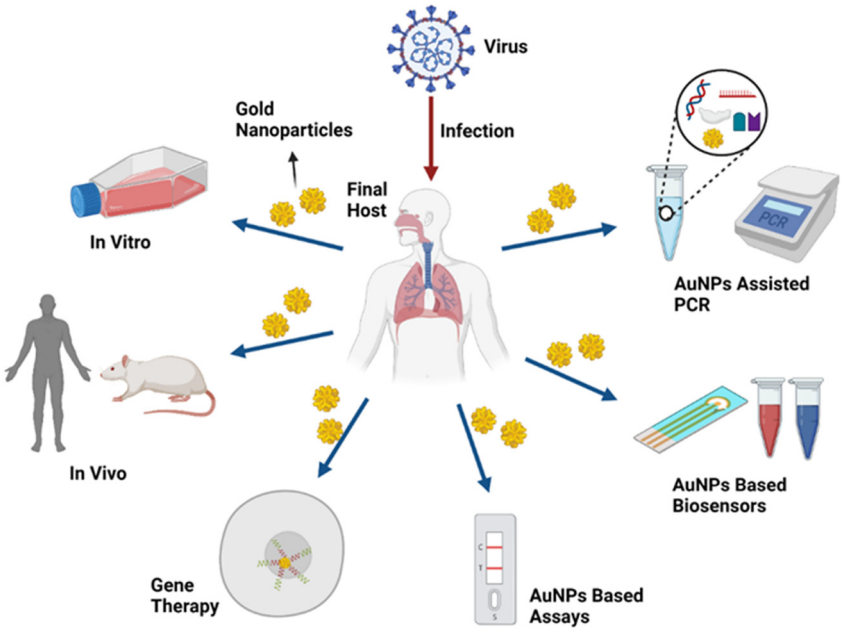

Figure 1: AuNPs against SARS-CoV-2: *in vitro* and *in vivo* studies, AuNP-assisted PCR, biosensors, lateral flow analysis, and gene therapy.

Table 1: *In vitro* and *in vivo* studies of AuNPs analyzed against the respiratory virus

Virus	NPs	Size (nm)	Concentration (time), administration route	Cell type/ model	Results	Ref.
SARS-CoV-2	AuNPs coated with SARS-CoV-2 S protein	10–100	—	—	The S-Au protein bind was demonstrated using the change of SPR band based on an external pH change	[145]
SARS-CoV-2	AuNPs-thiol-modified antisense oligonucleotides	55.4 ± 4.5	0.18 ng·μL^{-1}	Vero	AuNPs agglomerate selectively in the presence of the target RNA sequence of SARS-CoV-2. It was demonstrated in their SPR	[146]
SARS-CoV-2	NPs mixed with AuNPs: AgNPs, ZnONPs, and ClO_2	<40	0.01–0.425 ppm	Vero	NPs block viral entry by inhibiting the binding of SARS-CoV-2 S proteins to the ACE2 receptor	[147]
SARS-CoV-2	AuNPs-thiols and a new peptide	—	—	*In silico*	Notable effects on the SARS-CoV-2 receptor binding domain. Strong interaction with S protein. AuNPs-new peptide form was more stable	[34]
Influenza A	AuNPs FluPep	10	—	MDCK	FluPep-functionalized NPs have enhanced antiviral activity	[39]
Influenza A	AuNPs- sialic acid	2–14	—	MDCK	The high binding affinity of AuNPs to hemagglutinin is located on the virus surface	[40]
Influenza A	AuNPs	17 ± 2	0.5 μg·mL^{-1}	MDCK	Hemagglutination and virus infectivity was significantly inhibited	[148]
Influenza A	Porous AuNPs	154.24 ± 37.05	0.2 mg·mL^{-1}	MDCK	Notable decrease in viral replication. Strong affinity for disulfide bonds, which blocked the entry of the virus	[149]
Influenza H3N2	AuNPs-antibody specificity to influenza A	10	—	MDCK	Was observed a selective recognition of influenza H3N2 through a sensor	[150]
Respiratory syncytial virus RSV	Carboxylated AuNP-anti-RSV peptide	13	0.125–4 nM	HEp-2	The percentage of viral inhibition was 80–90%	[32]
RSV	Carboxylated AuNPs-dendrimer peptides	15	30 μg·mL^{-1}	HEp-2	The percentage of viral inhibition was 60 and 50% in already-infected cells	[42,43]
Rift Valley fever (RVF)	Spherical and rod-shaped AuNPs	20	40 μM	*In vitro, vivo:* Vero, rats	AuNPs can induce an autoimmune response after one dose	[43]

2 Antiviral activity of AuNPs on respiratory viruses

AuNPs' antiviral activity against viruses that cause respiratory diseases like SARS-CoV-2 is well known, and previous studies have particularly focused on certain viruses. Table 1 presents a summary of types of viruses for which AuNPs have been used. Regarding the selected *in vitro* studies that tested AuNPs' efficacy against SARS-CoV-2, some focused on the S protein and measured signal change *via* the SPR of the NPs (Figure 2). According to the crystalline structure analysis, the coronavirus has several key disulfide bonds, namely, Cys336–Cys361, Cys379–Cys432, and Cys391–Cys525. In particular, Cys480–Cys488 is a key in the junction between the virus crest and the N-terminal helix of ACE2 [36]. AuNPs, because of their chemical affinity with sulfur, could be coupled to the virus and thus stop viral replication [37].

Further, various studies have shown that COVID-19 can be treated using peptide inhibitors like heptad repeat 1 (HR1), which has been shown to inhibit HR1/HR2-mediated sheath merging between host cells and the Middle East respiratory syndrome coronavirus [38]. In one study, the peptide FluPep demonstrated excellent antiviral activity and efficiently inhibited influenza A viruses when functionalized with AuNPs [39]. In another study on the viral proliferation of influenza A using Madin-Darby canine kidney cells, the virus was effectively inhibited when viral hemagglutinin protein was targeted with AuNPs functionalized with sialic-acid-terminated glycerol dendrons, which was visually observed under electron microscopy imaging [40]. Many studies have also reported that AuNPs can significantly inhibit the proliferation of viruses by targeting the viral outer envelope [41]. In other studies with RSV [32] and RVF [42], viral inhibition of over 60% was observed [42], and in *in vivo* studies, an adequate immune response has been induced [43].

3 AuNP-assisted polymerase chain reaction

The RT-PCR technique amplifies a segment of the genetic material of interest and produces multiple copies. Thus, the PCR allows for the generation of millions of copies, or sometimes a single copy, of a particular nucleic sequence from an initial small sample. The PCR technique can be used as a molecular test to determine whether a virus's genetic material is present in the samples taken. In the case of severe and critical COVID-19 cases, the PCR test is highly accurate, sensitive, and specific [44]. However, more effective PCR results can be achieved by shortening the reaction time, increasing amplification efficiencies, and varying heating/cooling rates. For the latter, NPs can be used, as they have an essential role in heat transfer. Further, despite its many advantages, the PCR method may cause false-positive results owing to the long

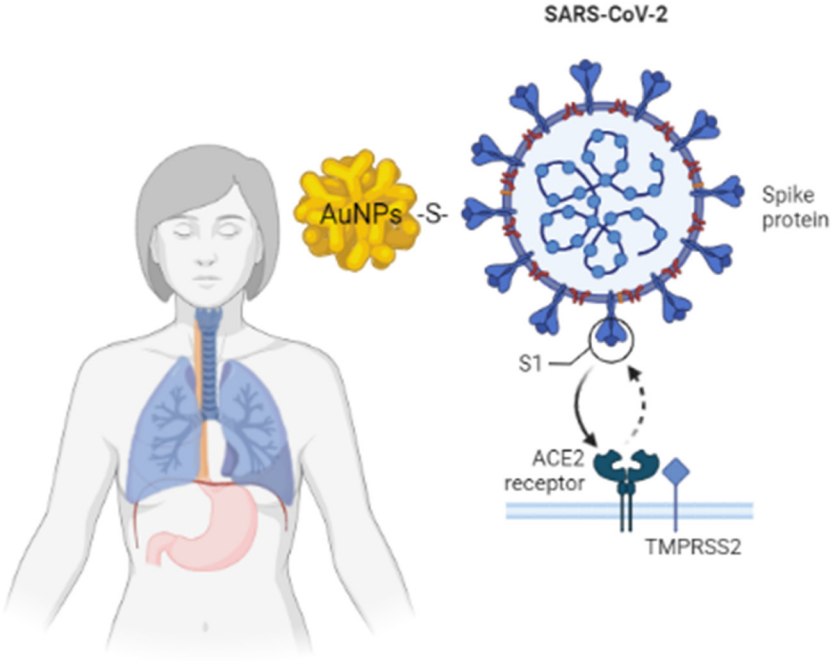

Figure 2: AuNPs mechanism against coronavirus SARS-CoV-2.

diagnostic time required and limited specificity; however, advancements in traditional methods, some of which have involved NPs, have reduced these false positives, and significantly decreased diagnostic time [45–47].

AuNPs are the most common NPs used in diagnosing viruses [31,48–50]. For example, AuNPs have been used to detect COVID-19 in a colorimetric PCR. In this hybrid method, AuNPs amplify the PCR to increase sensitivity, provide good visuals, and allow for *in situ* detection at a low cost thanks to properties including ionic force, pH, protein conformation, size, and shape [51]. Table 2 presents a summary of studies on AuNP-based PCR virus detection. Some of the studies that compared different PCR systems and found positive results for AuNPs showed that NPs did indeed significantly improve PCR results by at least 104%. Other studies also showed that AuNPs potentiated PCR products and could improve the test's specificity [52,53]. It was further found that AuNPs did not increase PCR specificity but instead suppressed the amplification of longer products while promoting the amplification of shorter products regardless of specificity [54]. After observing the surface interaction of AuNPs with PCR components, Lou and Zhang [55] found that interactions modulated the enzyme's binding with the template and primers during the reaction and thus lowered the melting temperature of the matching primers. Hamdy *et al.* [56] used an AuNP-assisted PCR test to detect foot and mouth disease virus (FMDV); they noted that NPs functionalized with FMDV-specific oligonucleotides increased the sensitivity and specificity of the typical PCR assay 10-fold. In terms of SARS-CoV-2, RT-PCRs were utilized to extract and partially purify RNA from saliva using the Boom (from Qiagen) approach and the sugar chain-immobilized AuNPs method. When compared to the standard Qiagen approach, the AuNPs method had a direct relationship with symptoms of mild or moderate COVID-19 in patients [57].

Some colorimetric methods in which AuNPs and globular nucleic acids act as binders have also been explored. In cases where the PCR technique cannot be applied on a large scale owing to insufficient resources and infrastructure, AuNPs can be used to visualize PCR products. This method prevents the single-component formation of spherical nucleic acids during the amplification process. Thus, positive and negative viral samples produce red and purple colors in the post-PCR colorimetric test [45,58,59]. It has also been found that larger-sized AuNPs can cause complete PCR inhibition at a lower particle concentration than smaller-sized AuNPs [45,60]. However, because the extent of AuNPs' effect on PCR efficiency is not clear, it is key that AuNPs studies be reviewed in detail and carried out using the correct dimensions.

Table 2: Gold nanoparticle-based PCR detections of viruses

Group/Virus	Target	AuNPs shape	AuNPs size (nm)	Biomolecule	Assay	Detection limit	Detection range	Detection platform	Time (min)	Ref.
Bunyaviridae hantaan virus (HTNV)	NC Protein	Spherical	30	DNA	IPCR	10 fg·mL^{-1}	105–1 fg·mL^{-1}	Microtitre plate	125	[151]
Retroviridae HIV	p24 antigen	Spherical	30	Antibody/DNA	IPCR	1 pg·mL^{-1}	10,000–1 pg·mL^{-1}	Microtiter plate	>125	[152]
Herpes virus-1 (EHV-1)	ND	Spherical	15	DNA	PCR	10^2	10^2–10^4	Microtiter plate	ND	[153]
Japanese encephalitis virus (JEV)	JEV genome	ND	13.2	DNA	PCR	ND	ND	Blood-Based PCR	ND	[154]
Respiratory syncytial virus	F-protein	ND	15	DNA/antibody	NPA-IPCR	4.1 PFU·mL^{-1}	ND	Microtitre plate	ND	[155]

Hence, AuNPs show promise for obtaining a more accurate DNA synthesis curve and improved reaction efficiency during real-time PCR analysis. The studies reviewed herein suggest that AuNPs will be very useful for future studies' advancement of PCR techniques.

4 AuNP-based biosensors

Given their simple production pathway, high plasmon resonance, excellent electrical/optical/catalytic properties, biocompatibility, and ability to simply detect antibodies, antigens, DNA, and RNA with 89–100% sensitivity, AuNPs are the most widely used metal NPs in biosensing applications for virus infections [61]. In general, AuNPs have mainly been used in second-generation biosensors because of their high surface-to-volume ratios, which improves the interaction between analyte and sensor. AuNP-based biosensors are classified into three main categories – electrochemical, piezoelectric, and optical biosensors (Table 3) – which are discussed in the following sections.

4.1 AuNP-based electrochemical biosensors

Electrochemical biosensors are frequently created using AuNPs, as they possess excellent catalytic properties, conductivity, and biocompatibility; they thus enhance electron transfer between redox centers of proteins, amplify electrode surfaces, and act as catalysts to increase electrochemical reactions. AuNPs also support electrochemical biosensing as they are highly biocompatible with easy protein functionality, and they improve transfer efficiency and surface-to-volume ratio [62]. The electrodes formed by AuNPs possess intrinsic metallic characteristics, resulting in excellent electrochemical behavior where free electrons migrate from the valence band to the conduction band. Nevertheless, it is essential to both biologically and chemically adjust NP surfaces when used with human specimens because of their high salt concentration. In the case of COVID-19, electrochemical biosensors, some of which have used AuNPs, have been successfully utilized to detect SARS-CoV-2.

4.2 AuNP-based piezoelectric biosensors

Research has found that analytical sensitivity can be improved by coupling the quartz crystal microbalance sensing process with AuNPs, as a high surface-to-volume ratio can amplify a mass charge on the crystals. Further, in many piezoelectric biosensors, AuNPs can enhance sensitivity and amplify signals; AuNPs facilitate rapid, sensitive detection by serving as an antibody carrier and mass enhancer in many sandwich-type immunosensors. In addition, piezoelectric biosensors possess a high potential to detect viruses from mechanical vibration or frequency changes by directly using output voltage. Piezoelectric biosensors have detected coronaviruses, HIV, and the viruses that cause hepatitis B, HPV, Ebola, vaccinia, influenza A, and dengue [63]. Interactions between DNA and the NP's surface (through electrons from bases, phosphate groups, or electrostatic forces) can influence both DNA's conformation and its electrical properties. Nanosensor materials containing AuNPs may aid in the creation of photonic equipment or biosensors for DNA detection in viruses such as SARS-CoV-2 [64].

4.3 AuNP-based optical biosensors

Colorimetric biosensors detect the presence of target biomarkers by causing the solution's color to change [65]. The AuNP-based colorimetric method for detecting nucleic acid was introduced by Mirkin using a DNA probe [66]. In this method, 30-nm nonaggregated AuNPs, in addition to functionalized magnet beads, are used for 60 min with a detection limit of 50 fmol·mL^{-1} to identify oligonucleotide sequences [67], which are detectable by color change *via* UV spectroscopy (Figure 3).

AuNPs are frequently used in optical bioassays because of their enhanced detection characteristics, including controlled fabrication, excellent visual performance, good biocompatibility, and particular catalytic activity. The central part of optical biosensors measures changes in photon or light output, and there are two types of detection methods: (1) indirect optical biosensors, in which a label (*e.g.*, chromophore or fluorophore) detects a binding event and amplifies the associated signal, and (2) direct optical biosensors, which function the same as SPR biosensors by detecting the change in the refractive index at the analyte–sensor interface [68].

AuNPs can be used in multiple optical sensing methods; one example is with the SPR that results from the interaction between conduction electrons in a metal and the electromagnetic wave. The primary function of SPR is to study and characterize the physicochemical changes of thin films on the metal surface [69]. Optical transducers have also been focused on by studies of Au nanostructures because of their plasmonic properties that produce interparticle

Table 3: Studies of Gold nanoparticle (AuNPs) base biosensors analyzed against respiratory viruses

Biosensors	Virus	NPs	Core-shell size	Objetive	Results	Ref.
Electro-chemical biosensor	SARS-CoV-2	Particular antisense oligonucleotides (ssDNA) capped with AuNPs	44.7 nm	The quantitative paper-based and rapid electrochemical biosensor chip were used to detect SARS-CoV-2 viral RNA in less than 5 min	In the presence of its target - SARS-CoV-2 RNA, a significant improvement in output signal was provided within less than 5 min of incubation time, with a detection limit of 6.9 copies per µL and a sensitivity of 231 copies per µL, with no further amplification	[156]
Electro-chemical biosensor	SARS-CoV-2	Fluorine doped tin oxide electrode (FTO) with AuNPs	—	eCovSens-Novel ultra-sensitive in-house built biosensor device (eCovSens) was used to compare with a commercial potentiostat to detect nCovid-19 spike antigen (nCovid-19Ag) in spiked saliva samples	eCovSens and FTO based immunosensor show high sensitivity for detecting nCovid-19Ag, varying from 1 fM to 1 µM. In standard buffer, nCovid-19Ag at 10 fM concentration can be successfully seen through an in-house developed device which is in close agreement with AuNPs/FTO sensor	[157]
Electro-chemical biosensor	MERS-CoV	Carbon electrodes (DEP) modified with AuNPs	50 nm	Development of a novel electrochemical immunosensor for the detection of coronavirus (MERS-CoV) using an array of AuNPs-modified carbon electrodes (DEP)	For MERS-CoV and HCoV, an excellent linear response was observed between the sensor response at the concentrations from 0.001 to 100 ng·mL^{-1} and 0.01 to 10,000 ng·mL^{-1}	[158]
Piezoelectric biosensors (QCM)	Dengue virus	Oligonucleotide functionalized with AuNPs	2 PFU·mL^{-1}	AuNPs layer-by-layer hybridization in a surface of quartz crystal microbalance (QCM) DNA sensing for the detection of dengue virus	The dengue viral RNA was detected in virus-contaminated serum through DNA-QCM biosensing when plaque titers were 2 PFU·mL^{-1} and a linear correlation range between 2 and 2 × 10^{6} PFU·mL^{-1}	[63]
Optical biosensors	Porcine Reproductive and Respiratory Syndrome Virus	Quantum dots and AuNPs	—	Development and Utilization of optical biosensor and nanophotonic technology to detect Porcine Reproductive and Respiratory Syndrome Virus (PRRSV)	The developed sensors can efficiently detect PRRSV in solution with a detection limit of 3 particles per µL	[70]
Optical biosensors	SARS-CoV-2	AuNPs-citrate	15–38 nm	AuNPs to detect the sequences coding for the RdRp, E, and S proteins of SARS-CoV-2	Detection limit ≥10^{3}–10^{4} viral RNA copies per µL	
Opto-microfluidic sensing	SARS-CoV-2	Au spikes	1 µg·mL^{-1}	An Opto-microfluidic sensing platform was developed with electrodeposition of gold nanospike to detect antibodies against SARS-CoV-2 spike protein	A detection limit of 0.5 pM in 30 min. was achieved by the developed sensing platform that falls under the clinically relevant concentration range. The Opto-microfluidic platform offers excellent potential for serological assays and promotes faster, cheap and easy SARS-CoV-2 diagnosis	[71]

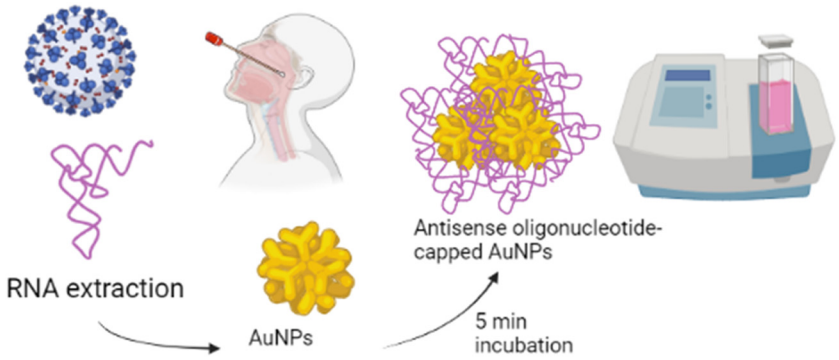

Figure 3: Schematic representation of a colorimetric assay based on antisense oligonucleotide-capped with AuNPs.

distance and plasmonic coupling. In addition, optical biosensors have been developed for accurate and rapid identification and detection of target biomolecules.

Further, numerous limitations of laborious conventional methods can be overcome by employing NPs. For example, practical and sensitive detection assays have been developed using advanced NP-based detection strategies to quickly confirm respiratory virus infection [70,71].

Functionalized AuNPs with single-stranded DNA have also been used to detect the *human p53* gene, including its 12 point mutation. AuNPs also possess distinctive SPR properties with high molar coefficients that show color change and size dependency. The aggregation of AuNPs with an SPR of 20 nm results in a color shift from red to blue in a colorimetric assay at 520 nm [72]. In the labeled type of colorimetric method, DNA ligands attach directly to AuNPs *via* chemical linkages before detection. AuNPs with modified ligands have higher hydration-based interparticle repulsions and are more stable at high ionic strength than simple AuNPs [73]. The ideal AuNPs aggregation can be achieved using cross-linking and noncross-linking. AuNPs aggregation *via* the cross-linked method is performed by inducing the controlled assembly of ligand-functionalized AuNPs, which forms a hydrogen bond that overrides the interparticle repulsive force. Chandrawati and Stevens [74] showed that AuNPs with peptide conjugate can be used to observe the concentration of factor XIII during blood clotting. Further, a one-step method for the rapid detection of MDM2, p14, and p53 (oncoproteins) was developed by Retout *et al.* [75]; the peptide-modified AuNPs form a ternary complex with MDM2, resulting in a color change from red to blue. Some recent research has also reported DNA's effect on the diffusion of Au particles, which helps control the morphology of AuNPs. For example, Soh *et al.* presented a combined diagnostic method using DNA aptamers and colorimetric techniques through physical adsorption [76], while Alafeef *et al.* developed an AuNP-based RNA extraction-free nano-amplified colorimetric test for point-of-care detection of COVID-19 [77]. This method uses a unique dual-prong strategy that integrates plasmonic sensing with nucleic acid amplification to detect SARS-CoV-2 with 98.4–100% sensitivity and specificity in a concentration of 10 copies per µL. This colorimetric test can be visualized as a quantitative response in a handheld point-of-care device.

A recent colorimetric study employing AuNPs to identify SARS-CoV-2 used molecular beacon oligonucleotides. The flanking nucleotides stabilized the oligonucleotide structure and enabled the selective identification of target sequences in the viral genome in 2.5 h with the naked eye, with an amplification of $\geq 10^3$–10^4 viral RNA copies per µL [78].

5 AuNP-based lateral flow assays for COVID-19 detection

The NP-based LFA is an easy-to-use, rapid, sensitive, and robust method to detect COVID-19 (Table 4) [79]. In an LFA, an analyte first reacts with labeled antibodies and moves further through the membrane by capillary force to the test and control zones and binds to captured antibodies [80].

AuNPs are extensively used in LFAs because of their bioconjugation, optically tunable, and plasmonic properties. AuNPs function as labels in LFAs and visualize results as red-colored lines. To increase LFA sensitivity, AuNPs have been decorated with silica nanorods [81]. To detect COVID-19, Khlebtsov and Khlebtsov [82] demonstrated an LFA incorporating visual color detection that used AuNPs in low concentrations (between 6.5×10^7 and 1.4×10^5 NPs·mm^{-2}) in a nitrocellulose membrane with a pore size of 10 µM. Serebrennikova *et al.* [83] reported an LFA that

Table 4: Some Commercially available lateral flow kits for COVID-19 detection

Lateral flow test kit type	Sample and detection type	Detection method	Sensitivity (%)	Testing time (min)	Ref.
BinaxNOW COVID-19 Ag Card, Abbott Diagnostics Scarborough, Inc	Nasal swab/N protein detection	Visual	100	15	[159]
CareStart COVID-19 Anti-gen test, Access Bio, Inc	Nasal swab/N protein detection	Visual detection	100	10	[160]
Lumira Dx SARS-CoV-2 Ag Test, Lumira Dx UK Ltd	Nasal swab/N protein detection	Fluorescence	96	12	[161]
Sofia 2 Flu + SARS Antigen Flow Immunoassay, Quidel Corporation	Nasal swab/N protein detection	Fluorescence	99	15	[162]
Biohit SARS-CoV-2 IgM/IgG Antibody Test Kit, Biohit Healthcare (Hefei) Co., Ltd	Serum, plasma, whole blood/Antibody detection (IgM and IgG)	Visual	96.7	10–20	[163]
COVID-19 IgG/IgM Rapid Test Cassette, Healgen Scientific LLC	Serum, plasma, whole blood/Antibody detection (IgM and IgG)	Visual	100	10	[164]
Diagnostic Kit for IgM/IgG Antibody to Coronavirus (SARS-CoV-2), Zhuhai Livzon Diagnostics Inc	Serum, plasma, whole blood/Antibody detection (IgM and IgG)	Visual	90.6	15	[165]
qSARS-CoV-2 IgG/IgM Rapid Test, Cellex Inc	Serum, plasma, whole blood/Antibody detection (IgM and IgG)	Visual	93.8	15	[166]
Sienna-Clarity COVIBLOCK COVID-19 IgG/IgM Rapid Test Cassette, Salofa Oy	Serum, plasma, whole blood/Antibody detection (IgM and IgG)	Visual	93.3	15–20	[165]
SARS-CoV-2 IgG IgM Antibody Rapid Test Kit, Lumigenex Co., Ltd	Serum, plasma, whole blood/Antibody detection (IgM and IgG)	Visual	100	15	[167]
SARS-CoV-2 Antibody Test, Guangzhou Wondfo Bio-tech Co., Ltd	Serum, plasma, whole blood/Antibody detection (IgM and IgG)	Visual	86.4	15	[168]
RapCov Rapid COVID-19 Test, ADVAITE, Inc	Serum, plasma, whole blood/Antibody detection (IgM and IgG)	Visual	90	10–20	[169]
Rapid COVID-19 IgM/IgG Combo Test Kit, Megna Health, Inc	Serum, plasma, whole blood/Antibody detection (IgM and IgG)	Visual	100	10	[170]

was five times as sensitive using hierarchical AuNPs in place of spherical AuNPs, while Zhang *et al.* [84] reported a limit of detection that was 100 times lower than normal using tipped flower-shaped AuNPs. Huang *et al.* [85] found that AuNP-LFA strips were more sensitive, specific, and stable in testing for COVID-19 in both positive and negative samples; further, the entire testing process required only 15 min compared to the various hours needed for PCR results, and only a minimum concentration of 10–20 μL was required. However, AuNP-LFA performance in COVID-19 testing depended on AuNPs' protein coating concentration and the block effects of the nitrocellulose membrane. Tests were performed with different concentrations (*i.e.*, 0.3, 0.6, 1.0, 1.2 mg·mL^{-1}) of SARS-CoV-2 AuNPs coated on the test; for positive tests, the brightest intensity of the test line corresponded to 1.2 mg·mL^{-1}. In another study, Cavalera *et al.* [86] developed a multitarget LF strip that could detect complete antibodies (IgG, IgM, and IgA) and the nucleocapsid protein of SARS-CoV-2. LF strips with AuNPs achieved 94.6% sensitivity and 100% specificity regarding the identification of IgA, which is produced earlier and at more detectable levels than IgG after SARS-CoV-2 infection. Thus, AuNP-based LF strips are more sensitive and provide results within minutes, making detection of COVID-19 faster and easier at point-of-care testing.

6 AuNP-based nucleic acid assays

The World Health Organization recommends the nucleic acid-based assay for COVID-19 testing as it is very specific and sensitive. This test depends on hybridization between probes and target, resulting in stable paring. This assay can also incorporate AuNPs: In the AuNPs-based nucleic acid assay, NPs are created using bifunctional ligands that bind as moieties on the particle's surface [87]. Nucleic acid assays using AuNPs can be divided into different categories based on the approach used for detection, as follows: (1) the AuNP-based sol-particle immunoassay, (2) the cross-linking approach using functionalized AuNPs, and (3) the noncross-linking approach [88].

7 AuNP-based approaches in DNA hybridization

DNA hybridization-based biosensors have enormous potential for disease diagnostics and forensic applications because of their speed, low cost, sensitivity, and suitability for point-of-care testing. Metal NPs like AuNPs are characterized by optical and electrical properties that are excellent for use in biosensors to identify DNA hybridization. Further, the use of enzyme-linked DNA probes and luminance-measuring labels has been incorporated into recently developed diagnostic approaches using AuNPs, also known as chemiluminescence [89]. For example, Li *et al.* aggregated AuNPs with different concentrations of NaCl, which facilitates label-free DNA hybridization detection [21]. This method does not require DNA strand labeling or a strict stripping procedure for AuNPs, which reduces the use of poisonous substances, and the separate hybridization steps under optimal laboratory conditions can detect target DNA strands as low as 1.1 fM [90]. In another study, Li and Rothberg used unlabeled or modified AuNPs for DNA hybridization detection between single-strand DNA probes and target DNA, resulting in AuNPs aggregation visible to the naked eye or with UV spectroscopy; it was found to be more sensitive than the labeled DNA probe [91]. Li and Rothberg developed a new approach for detecting target DNA in a homogenous solution based on an AuNPs light-scattering assay; it can be considered a one-step detection technique for DNA hybridization [92]. The light-scattering technique is unique in that it can detect a base change in DNA without temperature control. It is a simple, sensitive tool for AuNPs aggregation detection in a homogenous solution and provides a path for simpler and more specific DNA hybridization detection using AuNPs [93]. Thus, the research demonstrates that many metal NPs have been developed for medical applications; while all have their benefits, AuNPs are found to be ideal for COVID-19 diagnosis.

8 AuNP-based approaches for gene therapy

Regarding the effects of AuNPs in gene therapy, methods utilizing antisense oligonucleotides (ASOs) and peptide nucleic acids (PNAs) as therapeutic agents have attracted scholarly attention. ASOs activate and modulate RNA function in cells *via* different mechanisms. As the coupling between ASOs and mRNA becomes a substrate, the mRNA cannot be transported to the cytoplasm, and protein production is inhibited [94]. ASO treatment can be applied to target viral RNA; it has been shown to be a successful method for many diseases such as neurodegenerative and cardiological diseases [95,96]. In addition, ASOs have been used in many human subject studies to determine their clinical suitability,

and they have shown high efficacy against viral infections [45,97–99]. ASOs can easily be directed against the viral RNA of interest, impairing viral expansion, including SARS-CoV-2. Oligonucleotides bind to the targeted RNA and inhibit ASO translation [100].

Nevertheless, PNA's slow cellular uptake into cells is a challenge that needs to be overcome. This slow uptake may be because negatively charged phosphate backbones tend to fold into complex structures due to affinity. The hydrophobicity state causes PNA aggregation and nonspecific adhesions, and this folding tendency poses several limitations to this technology [101]. However, nanotechnological structures can assist PNAs at this stage: PNAs combined with AuNPs create more biocompatible candidates with lower toxicity and greater biodistribution, and AuNPs' tunable properties and accessible synthesis are further advantages. A study on antisense treatment for bovine viral diarrhea virus, which is a surrogate model of the human hepatitis C virus, showed that AuNPs are the most suitable method to provide PNAs to cells, which could lead to a potential tool for virus removal from infected cells [102].

Further, in 2020, Moitra *et al.* detailed a colorimetric test based on AuNPs coated with appropriately designed thiol-modified ASOs specific to the *N*-gene (nucleocapsid phosphoprotein) of SARS-CoV-2. The test could be used to diagnose positive COVID-19 cases from isolated RNA within 10 min. AuNPs, one of the ASO delivery systems, offer several advantages, including being able to bind to various types of molecules, low toxicity, and a broader absorption spectrum than other NPs [103]. No detailed studies have been conducted on using PNAs to disrupt the viral life cycle of SARS-COV-2 [104].

9 AuNP-based approaches in vaccine development

The application of nanotechnology in vaccines, known as nanovaccinology, is a growing field that focuses on enhancing the body's immune responses. NPs have been used in various ways, for example, to transport antibody-triggering antigens or make them more potent. AuNPs are a popular building block for nanovaccines because they are inert in the body and easily absorbed by specific immune cells. They have previously been used as carriers or enhancers in nanovaccine research and have also attracted medical attention for their antimicrobial and anti-inflammatory properties [101]. Intense research efforts resulted in the first vaccine candidate for COVID-19, which was tested in a Phase I clinical trial on March 16, 2020 [105]. By May 22, 2020, 10 COVID-19 vaccines were in human clinical trials, while 114 were still in preclinical development [106]. Vaccine development relies on the direct administration of viral protein antigens (*e.g.*, recombinant proteins, whole inactivated or attenuated virus, or vectored vaccines) or RNA or DNA that encodes viral antigens. The antigen candidate that induces immunization is the immunogenic spike protein (S1 subunit). As the S1 protein is essential for cellular uptake of the virus particle, many researchers concentrate on this protein as the primary target for a vaccine [107].

Conventional vaccines, such as inactivated, live attenuated viral, or subunit vaccines, possess certain limitations; for instance, there is a potential risk of viral virulence reversion (live attenuated viral vaccines) or weak immune response (inactivated viruses), as well as limited immunogenicity (subunit vaccines). However, recent advances in biological engineering have led to the design of nanotechnology-based vaccines that generate enhanced antigen presentation and strong immunogenicity [108]. NPs can assist in different ways to boost stimulation of the immune system and precisely direct the immune response against antigens [109].

There are different ways to deliver protein, drug, or RNA into a patient, but certain challenges, such as the vehicle often being degraded or swiftly cleared, impede successful delivery. NPs in the form of nanocarriers have the potential to overcome some of these limitations. For example, lipid-based, polymetric, or inorganic NPs could be manipulated to encapsulate cargo proteins with better protein delivery and pharmacokinetics than conventional methods [110]. In addition, intranasal application of encapsulated antigens has been found to induce a robust immune response; however, vaccine effectiveness depended on employing a suitable polymer compound with the antigen [111].

The target goal for most vaccines is to stimulate the production of the S protein [112]. For example, SARS vaccine research focused on S protein subunits, the receptor-binding domain of the S1 subunit, and the S protein/gene as the primary target sites [113,114]. Farfán-Castro *et al.* conducted one of the few studies on the use of AuNPs in vaccines, using a SARS-CoV-2 peptide with SH-PEG-NH2; the approach showed increased immunogenicity and cytokine production in mouse models, supporting the efficacy of nanovaccines in the battle against COVID-19 [115].

10 AuNP toxicity

Of all NPs, AuNPs have been most frequently used as vaccine platforms, as they are easily internalized by

macrophages and dendritic cells, which induce their activation [116]. Their ease of conjugation to biopolymers has allowed them to be used in cosmetic products, biological markers, biosensors, and theranostics, such as thermal ablation of tumors, radiation sensitizers, and real-time imaging *in vivo* and *in vitro* [117]. The advantage of AuNPs is that in their colloidal form, they do not accumulate in the liver. According to reports, they also do not cause liver dysfunction in *in vivo* or *in vitro* models [118]. Polyethylene glycol (PEG)-coated AuNPs, on the other hand, are protected from absorption by phagocytes and can be gradually eliminated from the body or degraded within cells [118,119].

In *in vivo* models using rats, AuNPs ranging in size from 5 to 100 nm were added intraperitoneally in concentrations from 5 to 20 $\mu g \cdot kg^{-1}$, orally from 20 to 1,300 $\mu g \cdot kg^{-1} \cdot day^{-1}$, and intravenously from 0.9 to 90 µg per rat. The reported effects ranged from low toxicity to oxidative damage in the lungs, renal tubule damage, increased pro-inflammatory cytokines, and lipid peroxidation in the liver [120–123]. In rabbit models, added AuNPs ranged in size from 5 to 25 nm and concentrations from 300 to 1,000 $\mu g \cdot kg^{-1}$ and were applied intravenously. The models were exposed from a minimum of 12 h to a maximum of 7 days and showed excellent results associated with mild toxicity such as inflammatory reactions in liver, lung, and kidney tissues; morphological or histological changes were not evident [124–126]. In an *in vitro* study of pulmonary 3D models, AuNPs toxicity was found. Their size varied from 15 to 175 nm, and the dose ranged from 40 to 500 $\mu g \cdot mL^{-1}$. The results demonstrated that size and material affected AuNPs' toxicological potential [127].

Regarding the metabolization of Au and its potential application in humans, studies carried out in patients with rheumatoid arthritis examining the dose and course of treatment of Au salts and articular morphology showed low toxicity [128–130]. Freyberg *et al.* [131] analyzed the dose of total Au ingested and plasma and urinary volume according to different intake schedules. They found the salts were not stored in the synovial fluid; their excretion was mainly hepatobiliary, approximately >70%, with secondary pathways including renal, skin, and breast tissue during pregnancy, and plasma values remained high after intake. It has also been shown that Au is distributed in the liver, kidney, spleen, hematopoietic tissues, bone, skin, adipose tissue, and eyes but does not reach the brain or skeletal muscle [132]. Biochemical analyses have shown that Au ions induce and bind to low-molecular-weight metalloproteins, albumins, alpha globulins, and histones in distributed tissues, with albumins and metalloproteins being the most abundant; in both cases, Au binds to free thiol groups in cysteine residues [133]. Au has a low affinity for keratogenic tissues; high levels are deposited in the dermis and connective tissues. Rarely, skin pathology resulting from prolonged contact with Au has been reported. However, there are millions of cases of allergic dermatitis from Au rings. In addition, Au can easily be removed by natural flaking of superficial squamous cells or natural growth in hair follicles or nail beds. Au particles have also been deposited in the corneal stroma, lens, conjunctiva, Descemet's and Bowman's membranes, and retina.

In cases of inhalation of Au dust from mines by humans, effects on the respiratory tract, stomach, and liver have been reported; only 15 min of exposure was needed to trigger a respiratory condition [134]. Further, Kusiak *et al.* analyzed post-mortem samples from more than 54,000 miners in Ontario between 1955 and 1986 and found a correlation with the occurrence of lung carcinoma [135]. Another study conducted on gold miners in Australia, the Americas, and South Africa found an association between stomach, liver, and respiratory tract cancer in people with alcoholism, smoking, localized diseases, and HIV [136]. The evidence is unclear regarding whether Au exposure is related to the occurrence of some specific cancer types; nevertheless, it has been confirmed that it is not mutagenic or genotoxic [137].

AuNPs toxicity is generally associated with particle size, surface coating [138], and shape. These specific aspects lead to different chemical attributes, some of which cellular research has shown to be toxic and others nontoxic. In addition, research has shown that the organ distribution of AuNPs is size dependent. For example, small AuNPs (5–15 nm) were more widely distributed among organs than larger AuNPs (50–100 nm), with the liver and spleen being the major targeted organs [139]. AuNPs' cytotoxicity in human cells has also been examined in detail, and studies have shown these NPs were nontoxic up to 250 mM, while ionic Au had a cytotoxicity at 25 mM [140].

The toxicity and biodistribution of PEG-coated AuNPs have also been studied. Results have indicated that AuNPs measuring 20 nm and coated with thioctic acid (TA)-terminated PEG5000 were the most stable and had the lowest toxicity among the 20-, 40-, and 80-nm AuNPs covered with TA-terminated PEG_{5000} [141]. While the toxicity of some AuNPs has been found to be size dependent due to their ligand surface coating [142], in others, their large surface-to-volume ratio provided an avenue for enhanced surface particle activity [143].

AuNPs' interactions with biological systems are mostly associated with their physicochemical characteristics, which allow them to be internalized within cells, unlike larger particles. Greater doses of AuNPs may be more toxic than those of larger particles, which indicates the relevance of their size, considering their high surface-to-volume ratio, for

Table 5: Studies evaluating AuNPs toxicity

Animal model	Surface coating	Size	Shape	Exposure: dose/Concentration	Main results	Ref.
Mice	PEG	13 nm	Spherical	Intravenous; Single injection of 170, 850, or 4,260 $\mu g \cdot kg^{-1}$	Acute inflammation and apoptosis by AuNPs were observed in the liver in a dose-dependent manner for 850 and 4,260 $\mu g \cdot kg^{-1}$	[171]
Mice	PEG	4 and 100 nm	Spherical	Intravenous; A single injection of 4,260 $\mu g \cdot kg^{-1}$	The PEG-AuNPs influenced apoptosis, cell cycle, inflammation, and metabolic processes in the liver. No histopathological changes in the liver	[141]
Mice	PEG	5, 10, 30 and 60 nm	Spherical	Intraperitoneal; a single dose of 4,000 $\mu g \cdot kg^{-1}$	Damage to the liver with 10 and 60 nm, as revealed by significant increases in the activities of ALT and AST; damage to the kidney with 60 nm, as shown by the significant decrease in the level of CREA; increased WBC and RBC count in 10 and 60 nm indicates an inflammatory response and effect on the hematopoietic system, respectively	[138]
Mice	PEG	15 nm	Spherical	Intravenous; a single dose of 5,000 $\mu g \cdot kg^{-1}$	Liver damage was observed	[172]
Mice	PEG	4.4, 22.5, 29.3 and 36.1 nm	Spherical	Intraperitoneal; 4,000 $\mu g \cdot kg^{-1}$	More significant liver toxicity in male mice is revealed by substantial increases in ALT and AST levels; possibilities of infection in male mice, as indicated by significant increases in WBC and RBC counts; no important toxicological response in the reproductive system in both female and male mice	[173]
Mice	PEG	10, 30 and 50 nm	Spherical	Intravenous; 400 $\mu g \cdot kg^{-1} \cdot day^{-1}$ for 14 days	No effect on systolic cardiac function, and no cardiac fibrosis or infiltration of inflammatory cells by the three sizes; 10 nm AuNPs for two weeks resulted in reversible cardiac hypertrophy, 30 and 50 nm AuNPs did not affect cardiac size over 12 weeks; administration of 50 nm AuNPs for 12 weeks decreased the synthesis of collagen, while 10 and 30 nm AuNPs did not affect collagen synthesis	[174]
Mice	Citrate	3, 5, 8, 17, 12, 37, 50, and 100 nm	Spherical	Intraperitoneal; 8,000 $\mu g \cdot kg^{-1} \cdot week^{-1}$	The 3- and 5-nm size AuNPs and 50–100 nm did not produce toxicity, But 8–37 nm induced death, with abnormalities in the liver, spleen, and lung	[175]
Mice	Citrate	10 nm	Spherical	Intraperitoneal; 2.5 × 104, 5 × 104, and 1 × 105 $\mu g \cdot kg^{-1} \cdot day^{-1}$	Significant increase in the RBC count and AST levels in the 5 × 104 $\mu g \cdot kg^{-1} \cdot day^{-1}$, which is an indication of toxicity	[176]
Mice	Citrate	13.5 nm	Spherical	Oral, intraperitoneal and intravenous; 1,100 $\mu g \cdot kg^{-1} \cdot day^{-1}$	The highest toxicity was observed in oral and intraperitoneal administration routes, while the	[177]

(Continued)

Table 5: *Continued*

Animal model	Surface coating	Size	Shape	Exposure: dose/Concentration	Main results	Ref.
					intravenous (tail vein) course showed the lowest toxicity	
Mice	Citrate	13.5 nm	Spherical	Oral; 200 µL at 137.5, 275, 550, 1,100, and 2,200 $\mu g \cdot kg^{-1} \cdot day^{-1}$	Decreased body weight, RBC levels, and HCT were observed at high concentrations (550–1,100 $\mu g \cdot kg^{-1}$). There was no apparent toxicity at low concentrations (137.5–275 $\mu g \cdot kg^{-1}$)	[177]
Mice	Citrate	21 nm	Spherical	Intraperitoneal; a single dose of 7,850 $\mu g \cdot kg^{-1}$	No detectable toxicity to vital organs; results correlated with significant fat loss and inhibition of inflammatory effects	[178]
Mice	Citrate	12.5 nm	Regular	Intraperitoneal; 40, 200, and 400 $\mu g \cdot kg^{-1} \cdot day^{-1}$	No evidence of toxicity was observed	[179]
Mice	Citrate	52.9 nm	Spherical	Oral; 0.2, 2 and 20 $mg \cdot kg^{-1} \cdot day^{-1}$	No toxicity was observed	[180]
Mice	Citrate	50 nm	Spherical	Acute: intravenous (single injection of 1,000, 2,000, and 10,000 $\mu g \cdot kg^{-1}$; chronic: intraperitoneal (1,000 and 2,000 $\mu g \cdot kg^{-1} \cdot day^{-1}$)	The toxicity was dose-, time-, and exposure frequency-dependent. Toxicity was observed in both exposures, especially with higher doses (2,000 and 10,000 $\mu g \cdot kg^{-1}$), while mortality was during the chronic study (2,000 $\mu g \cdot kg^{-1}$)	[181]
Mice	Tween 20	20 nm	Spherical	Intravenous; acute (single injection of 100, 250, 500, 750, 1,000, 1,250, 1,500, 1,750, and 2,000 $\mu g \cdot kg^{-1}$); subchronic (1,100 $\mu g \cdot kg^{-1} \cdot day^{-1}$)	There was no severe clinical or behavioral alteration in the acute toxicity test at all concentrations. In the subchronic test, it was found to be hepatotoxic	[182]
Rat	Porphyran	14 nm	Spherical	Oral; 375, 750 and 1,500 $ppm \cdot kg^{-1} \cdot day^{-1}$	Nontoxic and no abnormalities (in body weight, haematology or biochemical parameters) were recorded	[183]
Rat	N/R	10 and 50 nm	Spherical and hexagonal for 10 and 50 nm, respectively	Intraperitoneal; 5 µg/rat/day	10 nm AuNPs induced the highest toxicity in the liver and lung about time exposure. Size-dependent toxicity was noted	[184]
Rat	N/R	10 nm	N/R	Intraperitoneal; 5 µg/rat/day	Lipid peroxidation in the liver, but not in the heart and lungs	[120]
0	N/R	20 nm	N/R	Intraperitoneal; 20 $\mu g \cdot kg^{-1}$	There were induction of oxidative stress, impairment of glutathione peroxidase in rat brain, and decreased dopamine and serotonin levels	[185]
Rat	N/R	5–10 nm	Spherical	Intraperitoneal; 5-mL solution containing 5, 10, and 100 µg/rat/day	Damage to the renal tubules	[186]
Rat	N/R	10 and 50 nm	Spherical for 10 nm, hexagonal for 50 nm	Intraperitoneal; 22 $\mu g \cdot kg^{-1}$	Increased pro-inflammatory cytokines, which returned to normal after repeated exposure. The 50 nm AuNPs produced a more severe inflammatory response when compared to 10-nm AuNPs	[187]

(Continued)

Table 5: *Continued*

Animal model	Surface coating	Size	Shape	Exposure: dose/Concentration	Main results	Ref.
Rat	N/R	10, 20, and 50 nm	Spherical for 10 and 20 nm, and hexagonal for 50 nm	Intraperitoneal; 50 and 100 μL·day^{-1}	Changes in the hepatocytes, portal triads and the sinusoids; Nuclear destruction	[184]
Rat	Citrate	14 nm	Spherical	Intravenous; 0.9, 9, and 90 μg per rat (500 μL each)	No experimental acute or subchronic toxicity	[188]
Rat	Citrate	10–25 nm	N/R	Oral; 20 μg·kg^{-1}·day^{-1}	Toxic to the lung, liver, and kidney	[189]
Rat	Citrate	20 nm	Spherical	Intraperitoneal; 2,500 μg·kg^{-1}·day^{-1}	No observed toxicity with every 48-h administration. But 24-h administration showed marked parenchymal changes, necrosis and leukocyte infiltration	[190]
Rat	Citrate	5–15 nm	Spherical	Oral; 325, 650 and 1,300 μg·kg^{-1}·day^{-1}	No detectable toxicity	[191]
Rat	Citrate, CALNN	citrate-AuNPs: 16.1 ± 2.8 nm, CALNN-AuNPs: 16.3 ± 2.8	Spherical	Intravenous; single injection of ~0.7 mg·kg^{-1}	Significant decreases in HGB, HCT levels, and the number of RBCs, as well as spleen atrophy, were observed in rats injected with CALNN-AuNPs	[192]
Rat	Silica	100 nm	N/R	Intraperitoneal; single injection of 1,100 μg·kg^{-1} and exposure to the static magnetic field (1 h·day^{-1} for 14 day)	Oxidative damage was observed in rat lungs treated with AuNPs only, and more damage was observed when coexposed with a static magnetic field. This was due to the accumulation of AuNPs in the lung under a magnetic environment	[122]
Rabbit	Citrate	5 and 25 nm	Spherical	Intravenous; 1,000 μg·kg^{-1} single dose	No apparent acute toxicity	[125]
Rabbit	PEG	7 nm	Spherical	Intravenous; 300 μg·kg^{-1} single dose	There was no apparent acute toxicity, but inflammatory reactions in tissues, such as the liver, lungs, and kidneys, were observed	[124]
Rabbit	PEI2	N/R	N/R	Topical; 100 μL	No observed inflammation, redness, or edema in rabbit eyes, indicating a lack of toxicity of PEI2-AuNPs in corneal gene therapy	[126]
Zebrafish	Plain (spherical), CTAB, PSS, PAH (rods)	38.1 ± 2.8 nm (spherical), 12.7 ± 1.8 nm × 51.6 ± 8.2 nm (rods)	Spherical, rods	0.01, 0.025, 0.05, and 0.1 nM	No significant toxicity was observed with AuNSs at all doses tested. CTAB-AuNRs and PSS-AuNRs caused significant toxicity by high elevations in mortality and a decrease in hatching and heart rate. Additional coating with PAH further reduced the toxicity	[193]
Zebrafish	TMAT, MES and MEEE	1.5 nm	N/R	Waterborne; 100 μL, 0–250 μg·L^{-1}	Sublethal malformations were observed when exposed to MES-AuNPs, with no adverse responses on exposure to MEEE-AuNPs. Embryo mortality was induced by TMAT-AuNPs, with no mortality after exposure to MES- and MEEE-AuNPs. Pathways involved in inflammation and immune responses were affected	[194]

(Continued)

Table 5: *Continued*

Animal model	Surface coating	Size	Shape	Exposure: dose/Concentration	Main results	Ref.
Zebrafish	TMAT	1.3 nm	Spherical	Waterborne; 100 µL 80–5 × 104 µg·L^{-1}	Disruption of the progression of eye development and pigmentation, and embryonic mortality	[195]
Zebrafish	Mannose	16.5 ± 2.0 nm (spherical), 47.6 ± 3.0 × 12.3 ± 1.5 nm (Rod), 42.3 ± 2.5 × 16.1 ± 1.0 (nanostar)	Spherical, nanorod, and nanostar	Intraperitoneal; 2 µL contain five µg·g^{-1} single dose	No toxicity was observed up to 120 h	[196]
Zebrafish	Citrate	14 nm	Spherical	1.6 × 104 and 5.5 × 104 µg·kg^{-1} dry weight; 0.25 and 0.8 µg·L^{-1} released in water column	As well as increased activity of acetylcholinesterase, as well as modifications of genome composition, gene expressions, and DNA alterations, were observed	[197]
Broiler chicken	Gold(III) chloride hydrate (99.995%) HAuCl4	37.31 nm	Spherical	Lowest (5 ppm) and medium (15 ppm)	It caused recognizable oxidative damage to blood, histopathological changes, up-regulation of IL-6, expression of Nrf2 gene, fragmentation of DNA, a significant decrease in antibody titer against avian influenza and newcastle disease	[198]
Drosophila melanogaster	Citrate	5, 15, 40 and 80 nm	N/R	Dispersed in the food; 5, 15, 40 and 80 nm	Substantial reduction of Drosophila lifespan and fertility performance	[199]

their use in biomedical systems [144]. Most studies have focused on simple AuNPs (citrate or cetyltrimethylammonium bromide capped); thus, more research is needed on the toxicity and pharmacokinetics of functionalized AuNPs and should include accurate surface composition (*e.g.*, recognition and nonfouling molecules) since surface modifications can change the overall effect of the AuNPs.

Finally, most *in vivo* studies focused on intravenous injection as the main administration route of AuNPs. More investigation is required to evaluate the toxicity of AuNPs that include alternative means of AuNPs exposure, such as inhalation, oral absorption, and dermal absorption. Table 5 presents some of the studies that evaluated AuNPs toxicity.

Allometric scaling should be used as an empirical method for estimating the pharmacokinetic properties of pharmacological products in humans based on preclinical animal datasets during drug discovery and development, particularly to determine a safe initial dose for preliminary clinical trials.

11 Conclusions

This study reviewed the recent advances concerning AuNPs as an effective antiviral model, different methods of SARS-CoV-2 analysis with AuNPs, and their toxicity when used as a therapeutic strategy. Regarding the specific antiviral activity of AuNPs on SARS-CoV, viral replication inhibition occurs through NPs' binding with the SARS-CoV-2 S protein *via* its disulfide bridges owing to chemical affinity with Au. The same mechanism was reported for similar viruses such as influenza, RSV, and RVF, which support AuNPs' antiviral activity on respiratory viruses. In terms of utilizing AuNPs to detect respiratory viruses, with PCRs, the suggested size is 15–30 nm, the quantification limit for different viruses is 1 $fg{\cdot}mL^{-1}$, and for SARS-CoV-2, the amplification is $\geq 10^3$–10^4 copies of viral RNA per µL. When using electrochemical, piezoelectric, and colorimetric biosensors, AuNPs should measure 30–50 nm; electrochemical biosensors have the lowest detection limit (6.9 copies per µL) and optical biosensors approximately 0.5 $pg{\cdot}mL^{-1}$ in 30 min, while no studies have examined piezoelectric biosensors specifically for SARS-CoVo-2. For gene therapy approaches using isolated RNA ASOs, SARS-CoV-2 can be diagnosed in 10 min, which is the shortest analysis time compared to other techniques. The literature is scarce on the use of AuNPs in vaccines; however, using the SARS-CoV-2 peptide with SH-PEG-NH2 showed increased immunogenicity and cytokine production in mouse models, supporting the efficacy of a nanovaccine. Finally, the principal challenge associated with AuNPs application in illness diagnosis is their toxicity, namely, that it needs to be reduced and their bioavailability improved. Studies have shown that one advantage of using AuNPs is that they do not accumulate in the liver in humans in their colloidal form. In rats, AuNPs showed low toxicity, oxidative lung damage, renal tubule damage, increased pro-inflammatory cytokines, and lipid peroxidation in the liver. In *in vivo* models using rats, AuNPs (size: 5–100 nm) were added intraperitoneally in concentrations from 5 to 20 $\mu g{\cdot}kg^{-1}$, orally from 20 to 1,300 $\mu g{\cdot}kg^{-1}{\cdot}day^{-1}$, and intravenously from 0.9 to 90 µg per rat. In rabbit models, added AuNPs ranged in size from 5 to 25 nm and concentrations from 300 to 1,000 $\mu g{\cdot}kg^{-1}$ and were applied intravenously. In *in vitro* studies, size varied from 15 to 175 nm and dose from 40 to 500 $\mu g{\cdot}mL^{-1}$. Studies on toxicity in humans show AuNPs are excipient. Despite many studies on AuNPs, more research is required that evaluates their toxicity in terms of the various exposure routes, dose, and genetic effect over the long term.

Funding information: This study was funded by Pontificia Universidad Católica del Ecuador.

Author contributions: All authors have accepted responsibility for the entire content of this manuscript and approved its submission.

Conflict of interest: The authors state no conflict of interest.

Data availability statement: All data generated or analysed during this study are included in this published article.

References

[1] Mohan, B. and N. Vinod. COVID-19: An insight into SARS-CoV2 pandemic originated at Wuhan City in Hubei Province of China. *Journal of Infectious Diseases and Epidemiology*, Vol. 6, No. 4, 2020. id. 146.

[2] World Health Organization (WHO). *COVID-19 Weekly Epidemiological Update. Edition 47*, 2021.

[3] Ciotti, M., S. Angeletti, M. Minieri, M. Giovannetti, D. Benvenuto, S. Pascarella, et al. COVID-19 Outbreak: An Overview. *Chemotherapy*, Vol. 64, No. 5–6, 2019, pp. 215–223.

[4] Pilaquinga, F., J. Morey, M. Torres, and R. Seqqat. and M. de las N. Piña. Silver nanoparticles as a potential treatment against SARS-CoV-2: A review. *Wiley Interdisciplinary Reviews: Nanomedicine and Nanobiotechnology*, Vol. 13, No. 5, 2021, pp. 1–19.

[5] Pilaquinga, F., R. Bosch, J. Morey, C. Bastidas-Caldes, M. Torres, F. Toscano, et al. High *in vitro* activity of gold and silver nanoparticles from Solanum mammosum L. against SARS-CoV-2 surrogate Phi6 and viral model PhiX174. *Nanotechnology*, Vol. 34, No. 17, 2023.

[6] Raveendran, A. V., R. Jayadevan, and S. Sashidharan. Long COVID: An overview. *Diabetes & Metabolic Syndrome*, Vol. 15, No. 3, 2021, pp. 869–875.

[7] Wrapp, D., N. Wang, K. S. Corbett, J. A. Goldsmith, C. L. Hsieh, O. Abiona, et al. Cryo-EM structure of the 2019-nCoV spike in the prefusion conformation. *Science*, Vol. 367, No. 6483, 2020, pp. 1260–1263.

[8] Noman, A., M. Aqeel, N. Khalid, M. Hashem, S. Alamari, S. Zafar, et al. Spike glycoproteins: Their significance for corona viruses and receptor binding activities for pathogenesis and viral survival. *Microbial Pathogenesis*, Vol. 150, 2021, id. 104719.

[9] Tang, T., M. Bidon, J. A. Jaimes, G. R. Whittaker, and S. Daniel. Coronavirus membrane fusion mechanism offers a potential target for antiviral development. *Antiviral Research*, Vol. 178, 2020, id. 104792.

[10] Diamond, M., P. Halfmann, T. Maemura, K. Iwatsuki-Horimoto, S. Iida, M. Kiso, et al. The SARS-CoV-2 B.1.1.529 Omicron virus causes attenuated infection and disease in mice and hamsters. *Research Square*, 2021.

[11] Vangeel, L., W. Chiu, S. De Jonghe, P. Maes, B. Slechten, J. Raymenants, et al. Remdesivir, Molnupiravir and Nirmatrelvir remain active against SARS-CoV-2 Omicron and other variants of concern. *Antiviral Research*, Vol. 198, 2022, id. 105252.

[12] Tavakol, S., M. Zahmatkeshan, R. Mohammadinejad, S. Mehrzadi, M. T. Joghataei, M. S. Alavijeh, et al. The role of nanotechnology in current COVID-19 outbreak. *Heliyon*, Vol. 7, No. 4, 2021, id. e06841.

[13] Patra, J. K., G. Das, L. F. Fraceto, E. V. R. Campos, M. D. P. Rodriguez-Torres, L. S. Acosta-Torres, et al. Nano based drug delivery systems: recent developments and future prospects. *Journal of Nanobiotechnology*, Vol. 16, No. 1, 2018, pp. 1–33.

[14] Han, X., K. Xu, O. Taratula, and K. Farsad. Applications of nanoparticles in biomedical imaging. *Nanoscale*, Vol. 11, No. 3, 2019, pp. 799–819.

[15] Canaparo, R., F. Foglietta, F. Giuntini, C. Della Pepa, F. Dosio, and L. Serpe. Recent developments in antibacterial therapy: Focus on stimuli-responsive drug-delivery systems and therapeutic nanoparticles. *Molecules*, Vol. 24, No. 10, 2019, id. 1991.

[16] Carvalho, A. P. A. and C. A. Conte-Junior. Recent advances on nanomaterials to COVID-19 management: A systematic review on antiviral/virucidal agents and mechanisms of SARS-CoV-2 inhibition/inactivation. *Global Challenges*, Vol. 5, No. 5, 2021, id. 2000115.

[17] Park, J. E., K. Kim, Y. Jung, J. H. Kim, and J. M. Nam. Metal nanoparticles for virus detection. *ChemNanoMat*, Vol. 2, No. 10, 2016, pp. 927–936.

[18] Lin, L. C. W., S. Chattopadhyay, J. C. Lin, and C. M. J. Hu. Advances and opportunities in nanoparticle- and nanomaterial-based vaccines against bacterial infections. *Advanced Healthcare Materials*, Vol. 713, 2018, id. e1701395.

[19] Kanekiyo, M., C. J. Wei, H. M. Yassine, P. M. McTamney, J. C. Boyington, J. R. R. Whittle, et al. Self-assembling influenza nanoparticle vaccines elicit broadly neutralizing H1N1 antibodies. *Nature*, Vol. 4997456, 2013, pp. 102–106.

[20] Slütter, B., S. Bal, C. Keijzer, R. Mallants, N. Hagenaars, I. Que, et al. Nasal vaccination with N-trimethyl chitosan and PLGA based nanoparticles: Nanoparticle characteristics determine quality and strength of the antibody response in mice against the encapsulated antigen. *Vaccine*, Vol. 2838, 2010, pp. 6282–6291.

[21] Li, F., H. Zhang, B. Dever, X. F. Li, and X. C. Le. Thermal stability of DNA functionalized gold nanoparticles. *Bioconjugate Chemistry*, Vol. 2411, 2013, pp. 1790–1797.

[22] Ballester, M., C. Nembrini, N. Dhar, A. de Titta, C. de Piano, M. Pasquier, et al. Nanoparticle conjugation and pulmonary delivery enhance the protective efficacy of Ag85B and CpG against tuberculosis. *Vaccine*, Vol. 2940, 2011, pp. 6959–6966.

[23] Derakhshan, M. A., A. Amani, and R. Faridi-Majidi. State-of-the-Art of Nanodiagnostics and Nanotherapeutics against SARS-CoV-2. *ACS Applied Materials and Interfaces*, Vol. 13, No. 13, 2021, pp. 14816–14843.

[24] Joffre, O. P., E. Segura, A. Savina, and S. Amigorena. Cross-presentation by dendritic cells. *Nature Reviews Immunology*, Vol. 12, No. 8, 2012, pp. 557–569.

[25] Meka, R. R., S. Mukherjee, C. R. Patra, and A. Chaudhuri. Shikimoyl-ligand decorated gold nanoparticles for use in: *Ex vivo* engineered dendritic cell based DNA vaccination. *Nanoscale*, Vol. 11, No. 16, 2019, pp. 7931–7943.

[26] Sametband, M., I. Kalt, A. Gedanken, and R. Sarid. Herpes simplex virus type-1 attachment inhibition by functionalized graphene oxide. *ACS Applied Materials and Interfaces*, Vol. 6, No. 2, 2014, 1228-1235.

[27] Łoczechin, A., K. Séron, A. Barras, E. Giovanelli, S. Belouzard, Y. T. Chen, et al. Functional carbon quantum dots as medical countermeasures to human coronavirus. *ACS Applied Materials and Interfaces*, Vol. 1146, 2019, pp. 42964–42974.

[28] Naikoo, G. A., F. Arshad, I. U. Hassan, T. Awan, H. Salim, M. Z. Pedram, et al. Nanomaterials-based sensors for the detection of COVID-19: A review. *Bioengineering & Translational Medicine*, Vol. 7, No. 3, 2022, id. e10305.

[29] Mateo, D., P. Morales, A. Ávalos, A. Haza, and I. Ana. Gold nanoparticles: Applications and *in vitro* cytotoxicity. *Acta Toxicol Argent*, Vol. 21, No. 2, 2013, pp. 102–109.

[30] Sztandera, K., M. Gorzkiewicz, and B. Klajnert-Maculewicz. Gold nanoparticles in cancer treatment. *Molecular Pharmaceutics*, Vol. 16, No. 1, 2019, pp. 1–23.

[31] Draz, M. S. and H. Shafiee. Applications of gold nanoparticles in virus detection. *Theranostics*, Vol. 8, No. 7, 2018, pp. 1985–2017.

[32] Singh, S. R., P. M. Tiwari, and V. A. Dennis. *Anti respiratory syncytial virus peptide functionalized gold nanoparticles*. USA 8815295, 2014, pp. 1–7.

[33] Yafout, M., A. Ousaid, Y. Khayati, and I. S. El Otmani. Gold nanoparticles as a drug delivery system for standard chemotherapeutics: A new lead for targeted pharmacological cancer treatments. *Scientific African*, Vol. 11, 2021, id. e00685.

[34] Mehranfar, A. and M. Izadyar. Theoretical design of functionalized gold nanoparticles as antiviral agents against severe acute respiratory syndrome coronavirus 2 (SARS-CoV-2). *The Journal of Physical Chemistry Letters*, Vol. 1124, 2020, pp. 10284–10289.

[35] Paradowska, E., M. Studzińska, A. Jabłońska, V. Lozovski, N. Rusinchuk, I. Mukha, et al. Antiviral effect of nonfunctionalized gold nanoparticles against herpes simplex virus type-1 (HSV-1) and possible contribution of near-field interaction mechanism. *Molecules (Basel, Switzerland)*, Vol. 26, No. 19, 2021, p. 5960.

[36] Shi, Y., A. Zeida, C. E. Edwards, M. L. Mallory, S. Sastre, M. R. Machado, et al. Thiol-based chemical probes exhibit antiviral activity against SARS-CoV-2 via allosteric disulfide disruption in the spike glycoprotein. *Proceedings of the National Academy of Sciences of the United States of America*, Vol. 119, No. 6, 2022, id. e2120419119.

[37] Chung, Y. C., I. H. Chen, and C. J. Chen. The surface modification of silver nanoparticles by phosphoryl disulfides for improved biocompatibility and intracellular uptake. *Biomaterials*, Vol. 2912, 2008, pp. 1807–1816.

[38] Ahmed, S. R., É. Nagy, and S. Neethirajan. Self-assembled star-shaped chiroplasmonic gold nanoparticles for an ultrasensitive chiro-immunosensor for viruses. *RSC Advances*, Vol. 7, 2017, pp. 40849–40857.

[39] Alghrair, Z. K., D. G. Fernig, and B. Ebrahimi. Enhanced inhibition of influenza virus infection by peptide–noble-metal nanoparticle conjugates. *Beilstein Journal of Nanotechnology*, Vol. 10, 2019, pp. 1038–1047.

[40] Papp, I., C. Sieben, K. Ludwig, M. Roskamp, C. Böttcher, S. Schlecht, et al. Inhibition of Influenza Virus Infection by Multivalent Sialic-Acid-Functionalized Gold Nanoparticles. *Small*, Vol. 624, 2010, pp. 2900–2906.

[41] Rosemary Bastian, A., A. Nangarlia, L. D. Bailey, A. Holmes, R. V. Kalyana Sundaram, C. Ang, et al. Mechanism of multivalent nanoparticle encounter with HIV-1 for potency enhancement of peptide triazole virus inactivation. *Journal of Biological Chemistry*, Vol. 290, No. 1, 2015, pp. 529–543.

[42] Baganizi, D. R., S. Bawage, A. Singh, P. Tiwari, V. A. Dennis, and S. R. Singh. Peptide-functionalized gold nanoparticles are potent inhibitors of respiratory syncytial virus (RSV) infection. *Advanced Materials: TechConnect Briefs*, 2016, pp. 127–130.

[43] Abo Elqasem, A. and A. Mohamed. Influence of gold nanoparticles on the immune response to rift valley fever vaccine and related hepatophysiological toxicity, histological, and immunohistochemical alterations. *The Egyptian Journal of Pediatric Allergy and Immunology*, Vol. 19, No. 1, 2021, pp. 37–49.

[44] Long, C., H. Xu, Q. Shen, X. Zhang, B. Fan, C. Wang, et al. Diagnosis of the Coronavirus disease (COVID-19): rRT-PCR or CT? *European Journal of Radiology*, Vol. 126, 2020, id. 108961.

[45] Wan, W., J. T. W. Yeow, and M. I. Van Dyke. Size-dependent PCR inhibitory effect induced by gold nanoparticles. In: *Proceedings of the 31st Annual International Conference of the IEEE Engineering in Medicine and Biology Society: Engineering the Future of Biomedicine*. EMBC; 2009, 2009, pp. 2771–2774.

[46] Jung, H. S., G. J. Tsongalis, and J. A. Lefferts. Development of HLA-B*57:01 Genotyping real-time PCR with optimized hydrolysis probe design. *Journal of Molecular Diagnostics*, Vol. 19, No. 5, 2017, pp. 742–754.

[47] Dworkin, L. L., T. M. Gibler, and R. N. Van Gelder. Real-time quantitative polymerase chain reaction diagnosis of infectious posterior uveitis. *Archives of Ophthalmology*, Vol. 12011, 2002, pp. 1534–1539.

[48] Khan, M. S., G. D. Vishakante, and H. Siddaramaiah. Gold nanoparticles: A paradigm shift in biomedical applications. *Advances in Colloid and Interface Science*, Vol. 199–200, 2013, pp. 44–58.

[49] Dykman, L. A. and N. G. Khlebtsov. Gold nanoparticles in biology and medicine: Recent advances and prospects. *Acta Naturae*, Vol. 3, No. 2, 2011, pp. 34–55.

[50] Vanzha, E., T. Pylaev, V. Khanadeev, S. Konnova, V. Fedorova, and N. Khlebtsov. Gold nanoparticle-assisted polymerase chain reaction: effects of surface ligands, nanoparticle shape and material. *RSC Advances*, Vol. 6111, 2016, pp. 110146–110154.

[51] Wang, W., X. Wang, J. Liu, C. Lin, J. Liu, and J. Wang. The integration of gold nanoparticles with polymerase chain reaction for constructing colorimetric sensing platforms for detection of health-related DNA and proteins. *Biosensors*, Vol. 12, No. 6, 2022, p. 421.

[52] Sleczkowski, P., M. Borkowski, H. Zajaczkowska, J. Ulanski, W. Pisula, and T. Marszalek. Geometry control of source/drain electrodes in organic field-effect transistors by electrohydrodynamic inkjet printing. *Materials*, Vol. 1321, 2020, pp. 1–16.

[53] Li, M., Y. C. Lin, C. C. Wu, and H. S. Liu. Enhancing the efficiency of a PCR using gold nanoparticles. *Nucleic Acids Research*, Vol. 33, No. 21, 2005, id. e184.

[54] Vu, B. V., D. Litvinov, and R. C. Willson. Gold nanoparticle effects in polymerase chain reaction: Favoring of smaller products by polymerase adsorption. *Analytical Chemistry*, Vol. 80, No. 14, 2008, pp. 5462–5467.

[55] Lou, X. and Y. Zhang. Mechanism studies on nanoPCR and applications of gold nanoparticles in genetic analysis. *ACS Applied Materials and Interfaces*, Vol. 5, No. 13, 2013, pp. 6276–6284.

[56] Hamdy, M. E., M. Del Carlo, H. A. Hussein, T. A. Salah, A. H. El-Deeb, M. M. Emara, et al. Development of gold nanoparticles biosensor for ultrasensitive diagnosis of foot and mouth disease virus. *Journal of Nanobiotechnology*, Vol. 16, No. 1, 2018, id. 48.

[57] Kajiya, T., H. Sawayama, E. Arima, M. Okamoto, M. Baba, M. Toyama, et al. Novel RT-PCR using sugar chain-immobilized gold-nanoparticles correlates patients' symptoms: The follow-up study of COVID-19 hospitalized patients. *Viruses*, Vol. 14, No. 11, 2022, p. 2577.

[58] Karami, A., M. Hasani, F. Azizi Jalilian, and R. Ezati. Conventional PCR assisted single-component assembly of spherical nucleic acids for simple colorimetric detection of SARS-CoV-2. *Sensors and Actuators. B: Chemical*, Vol. 328, 2021, id. 128971.

[59] Karami, A., M. Hasani, F. Azizi Jalilian, and R. Ezati. Hairpin-spherical nucleic acids for diagnosing COVID-19: a simple method to generalize the conventional PCR for molecular assays. *Analytical Chemistry*, Vol. 93, No. 26, 2021, pp. 9250–9257.

[60] Wan, W. and J. T. W. Yeow. The effects of gold nanoparticles with different sizes on polymerase chain reaction efficiency. *Nanotechnology*, Vol. 2032, 2009, id. 325702.

[61] Bhavana, V., P. Thakor, S. B. Singh, and N. K. Mehra. COVID-19: Pathophysiology, treatment options, nanotechnology approaches, and research agenda to combating the SARS-CoV2 pandemic. *Life Sciences*, Vol. 261, 2020, id. 118336.

[62] Cho, I. H., J. Lee, J. Kim, M. soo Kang, J. Paik, S. Ku, et al. Current technologies of electrochemical immunosensors: Perspective on signal amplification. *Sensors*, Vol. 18, No. 2, 2018, id. 207.

[63] Chen, S. H., Y. C. Chuang, Y. C. Lu, H. C. Lin, Y. L. Yang, and C. S. Lin. A method of layer-by-layer gold nanoparticle hybridization in a quartz crystal microbalance DNA sensing system used to detect dengue virus. *Nanotechnology*, Vol. 2021, 2009, id. 215501.

[64] Akın, S., G. Karanfil, A. Gültekin, and S. Sönmezoğlu. Improvement of physical properties of CdO thin films by Au–Ag nanocluster codoping. *Journal of Alloys and Compounds*, Vol. 579, 2013, pp. 272–278.

[65] Truong, P. L., Y. Yin, D. Lee, and S. H. Ko. Advancement in COVID-19 detection using nanomaterial-based biosensors. *Exploration*, Vol. 3, No. 1, 2023, id. 20210232.

[66] Zhao, W., M. A. Brook, and Y. Li. Design of gold nanoparticle-based colorimetric biosensing assays. *ChemBioChem*, Vol. 915, 2008, pp. 2363–2371.

[67] Wu, S., D. Li, J. Wang, Y. Zhao, S. Dong, and X. Wang. Gold nanoparticles dissolution based colorimetric method for highly sensitive detection of organophosphate pesticides. *Sensors and Actuators, B: Chemical*, Vol. 238, 2017, pp. 427–433.

[68] Wang, R. and Y. Li. Biosensors for rapid detection of avian influenza. In: *Steps Forwards in Diagnosing and Controlling Influenza, Intechopen*, 2016, p. 61.

[69] Hu, M., J. Chen, Z. Y. Li, L. Au, G. V. Hartland, X. Li, et al. Gold nanostructures: Engineering their plasmonic properties for biomedical applications. *Chemical Society Reviews*, Vol. 3511, 2006, pp. 1084–1094.

[70] Stringer, R. C., S. Schommer, D. Hoehn, and S. A. Grant. Development of an optical biosensor using gold nanoparticles and quantum dots for the detection of Porcine Reproductive and Respiratory Syndrome Virus. *Sensors and Actuators B: Chemical*, Vol. 134, No. 2, 2008, pp. 427–431.

[71] Funari, R., K. Y. Chu, and A. Q. Shen. Detection of antibodies against SARS-CoV-2 spike protein by gold nanospikes in an opto-microfluidic chip. *Biosensors and Bioelectronics*, Vol. 169, 2020, id. 112578.

[72] Sabela, M., S. Balme, M. Bechelany, J. M. Janot, and K. Bisetty. A Review of Gold and Silver Nanoparticle-Based Colorimetric Sensing Assays. *Advanced Engineering Materials*, Vol. 19, No. 12, 2017.

[73] Buurma, N. J. and I. Haq. Advances in the analysis of isothermal titration calorimetry data for ligand-DNA interactions. *Methods*, Vol. 42, No. 2, 2007, pp. 162–172.

[74] Chandrawati, R. and M. M. Stevens. Controlled assembly of peptide-functionalized gold nanoparticles for label-free detection of blood coagulation Factor XIII activity. *Chemical Communications*, Vol. 5041, 2014, pp. 5431–5434.

[75] Retout, M., H. Valkenier, E. Triffaux, T. Doneux, K. Bartik, and G. Bruylants. Rapid and selective detection of proteins by dual trapping using gold nanoparticles functionalized with peptide aptamers. *ACS Sensors*, Vol. 1, No. 7, 2016, pp. 929–933.

[76] Soh, J. H., Y. Lin, S. Rana, J. Y. Ying, and M. M. Stevens. Colorimetric detection of small molecules in complex matrixes via target-mediated growth of aptamer-functionalized gold nanoparticles. *Analytical Chemistry*, Vol. 8715, 2015, pp. 7644–7652.

[77] Alafeef, M., P. Moitra, K. Dighe, and D. Pan. RNA-extraction-free nano-amplified colorimetric test for point-of-care clinical diagnosis of COVID-19. *Nature Protocols*, Vol. 16, No. 6, 2021, pp. 3141–3162.

[78] Rodríguez Díaz, C., N. Lafuente-Gómez, C. Coutinho, D. Pardo, H. Alarcón-Iniesta, M. López-Valls, et al. Development of colorimetric sensors based on gold nanoparticles for SARS-CoV-2 RdRp, E and S genes detection. *Talanta*, Vol. 243, 2022, id. 123393.

[79] Jain, P. K., X. Huang, I. H. El-Sayed, and M. A. El-Sayed. Noble metals on the nanoscale: Optical and photothermal properties and some applications in imaging, sensing, biology, and medicine. *Accounts of Chemical Research*, Vol. 4112, 2008, pp. 1578–1586.

[80] Azzazy, H. M. E., M. M. H. Mansour, and S. C. Kazmierczak. Nanodiagnostics: A new frontier for clinical laboratory medicine. *Clinical Chemistry*, Vol. 52, No. 7, 2006, pp. 1238–1246.

[81] Zhong, Y., Y. Chen, L. Yao, D. Zhao, L. Zheng, G. Liu, et al. Gold nanoparticles based lateral flow immunoassay with largely amplified sensitivity for rapid melamine screening. *Microchimica Acta*, Vol. 183, No. 6, 2016, pp. 1989–1994.

[82] Khlebtsov, B. and N. Khlebtsov. Surface-enhanced Raman scattering-based lateral-flow immunoassay. *Nanomaterials*, Vol. 1011, 2020, pp. 1–16.

[83] Serebrennikova, K., J. Samsonova, and A. Osipov. Hierarchical Nanogold Labels to Improve the Sensitivity of Lateral Flow Immunoassay. *Nano-Micro Letters*, Vol. 10, No. 2, 2018, p. 24.

[84] Zhang, L., Y. Huang, J. Wang, Y. Rong, W. Lai, J. Zhang, et al. Hierarchical flowerlike gold nanoparticles labeled immunochromatography test strip for highly sensitive detection of escherichia coli O157:H7. *Langmuir*, Vol. 31, No. 19, 2015, pp. 5537–5544.

[85] Huang, C., Y. Wang, X. Li, L. Ren, J. Zhao, Y. Hu, et al. Clinical features of patients infected with 2019 novel coronavirus in Wuhan, China. *The Lancet*, Vol. 395, No. 10223, 2020, pp. 497–506.

[86] Cavalera, S., B. Colitti, S. Rosati, G. Ferrara, L. Bertolotti, C. Nogarol, et al. A multi-target lateral flow immunoassay enabling the specific and sensitive detection of total antibodies to SARS COV-2. *Talanta*, Vol. 223, 2021, id. 121737.

[87] Thaxton, C. S., D. G. Georganopoulou, and C. A. Mirkin. Gold nanoparticle probes for the detection of nucleic acid targets. *Clinica Chimica Acta*, Vol. 363, No. 1–2, 2006, pp. 120–126.

[88] Algar, W., M. Massey, and U. J. Krull. The application of quantum dots, gold nanoparticles and molecular switches to optical nucleic-acid diagnostics. *TrAC - Trends in Analytical Chemistry*, Vol. 28, No. 3, 2009, pp. 292–306.

[89] Whitworth, M., L. Bricker, and C. Mullan. Ultrasound for fetal assessment in early pregnancy. *Cochrane database of systematic reviews*, John Wiley and Sons Ltd, UK, Vol. 2015, 2015.

[90] Qi, Y., B. Li, and Z. Zhang. Label-free and homogeneous DNA hybridization detection using gold nanoparticles-based chemiluiminescence system. *Biosensors and Bioelectronics*, Vol. 24, No. 12, 2009, pp. 3581–3586.

[91] Li, H. and L. Rothberg. Detection of specific sequences in RNA using differential adsorption of single-stranded oligonucleotides on gold nanoparticles. *Analytical Chemistry*, Vol. 77, No. 19, 2005, pp. 6229–6233.

[92] Li, H. and L. J. Rothberg. DNA sequence detection using selective fluorescence quenching of tagged oligonucleotide probes by gold nanoparticles. *Analytical Chemistry*, Vol. 76, No. 18, 2004, pp. 5414–5417.

[93] Du, B. A., Z. P. Li, and C. H. Liu. One-step homogeneous detection of DNA hybridization with gold nanoparticle probes by using a linear light-scattering technique. *Angewandte Chemie - International Edition*, Vol. 45, No. 47, 2006, pp. 8022–8025.

[94] Schubert, S. and J. Kurreck. Oligonucleotide-based antiviral strategies. In: *RNA Towards Medicine*, Springer Berlin Heidelberg, 2006, pp. 261–287.

[95] Sardone, V., H. Zhou, F. Muntoni, A. Ferlini, and M. S. Falzara. Antisense oligonucleotide-based therapy for neuromuscular disease. *Molecules*, Vol. 22, No. 4, 2017, id. 563.

[96] Leavitt, B. R. and S. J. Tabrizi. Antisense oligonucleotides for neurodegeneration. *Science*, Vol. 3676485, 2020, pp. 1428–1429.

[97] Lenartowicz, E., A. Nogales, E. Kierzek, R. Kierzek, L. Martínez-Sobrido, and D. H. Turner. Antisense oligonucleotides targeting influenza a segment 8 genomic RNA inhibit viral replication. *Nucleic Acid Therapeutics*, Vol. 26, No. 5, 2016, pp. 277–285.

[98] De Jong, Y. P. and I. M. Jacobson. Antisense therapy for hepatitis C virus infection. *Journal of Hepatology*, Vol. 60, No. 1, 2014, pp. 227–228.

[99] Chery, J., A. Petri, A. Wagschal, S. Y. Y. Lim, J. Cunningham, S. Vasudevan, et al. Development of locked nucleic acid antisense oligonucleotides targeting ebola viral proteins and host factor niemann-Pick C1. *Nucleic Acid Therapeutics*, Vol. 28, No. 5, 2018, pp. 273–284.

[100] Galderisi, U., A. Cascino, and A. Giorda. Antisense oligonucleotides as therapeutic agents. *Journal of Cellular Physiology*, Vol. 181, No. 2, 1999, pp. 251–257.

[101] Gupta, A., R. Bahal, M. Gupta, P. M. Glazer, and W. M. Saltzman. Nanotechnology for delivery of peptide nucleic acids (PNAs). *Journal of Controlled Release*, Vol. 240, 2016, pp. 302–311.

[102] Ghaffari, E., S. E. Rezatofighi, M. R. Ardakani, and S. Rastegarzadeh. Delivery of antisense peptide nucleic acid by gold nanoparticles for the inhibition of virus replication. *Nanomedicine*, Vol. 1414, 2019, pp. 1827–1840.

[103] Deanasa, R. S. D., P. M. A. Afladhanti, and F. Syafira. The potential of antisense oligonucleotides (ASO) through inhalation based on gold nanoparticle (AuNP) delivery system in inhibiting SARS-CoV-2 replication and transcription. *SCRIPTA SCORE Scientific Medical Journal*, Vol. 4, No. 1, 2022, pp. 82–91.

[104] Li, A. J., K. S. PhaChengxi, B. Callahandke, C. E. Bellaire, G. Farquhar, Zhang, et al. Automated Flow Synthesis of Peptide-PNA Conjugates. *ACS Central Science*, Vol. 8, No. 2, 2022, pp. 205–213.

[105] *NIH clinical trial of investigational vaccine for COVID-19 begins*. National Institute of Health, 2020.
[106] Draft landscape of COVID-19 candidate vaccines, 2020.
[107] Amanat, F. and F. Krammer. SARS-CoV-2 vaccines: status report. *Immunity*, Vol. 52, 2020, pp. 583–589.
[108] Jindal, S. and P. Gopinath. Nanotechnology based approaches for combatting COVID-19 viral infection. *Nano Express*, Vol. 1, No. 2, 2020, id. 22003.
[109] Weiss, C., M. Carriere, L. Fusco, L. Fusco, I. Capua, J. A. Regla-Nava, et al. Toward Nanotechnology-Enabled Approaches against the COVID-19 Pandemic. *ACS Nano*, Vol. 14, No. 6, 2020, pp. 6383–6406.
[110] Yu, M., J. Wu, J. Shi, and O. C. Farokhzad. Nanotechnology for protein delivery: Overview and perspectives. *Journal of Controlled Release*, Vol. 240, 2016, pp. 24–37.
[111] Nochi, T., Y. Yuki, H. Takahashi, S. I. Sawada, M. Mejima, T. Kohda, et al. Nanogel antigenic protein-delivery system for adjuvant-free intranasal vaccines. *Nature Materials*, Vol. 9, No. 7, 2010, pp. 572–578.
[112] Chauhan, G., M. J. Madou, S. Kalra, V. Chopra, D. Ghosh, and S. O. Martinez-Chapa. Nanotechnology for COVID-19: Therapeutics and Vaccine Research. *ACS Nano*, Vol. 14, No. 7, 2020, pp. 7760–7782.
[113] Prompetchara, E., C. Ketloy, and T. Palaga. Immune responses in COVID-19 and potential vaccines: Lessons learned from SARS and MERS epidemic. *Asian Pacific Journal of Allergy and Immunology*, Vol. 38, No. 1, 2020, pp. 1–9.
[114] Zhang, L. and Y. Liu. Potential interventions for novel coronavirus in China: A systematic review. *Journal of Medical Virology*, Vol. 92, No. 5, 2020, pp. 479–490.
[115] Farfán-Castro, S., M. J. García-Soto, M. Comas-García, J. I. Arévalo-Villalobos, G. Palestino, O. González-Ortega, et al. Synthesis and immunogenicity assessment of a gold nanoparticle conjugate for the delivery of a peptide from SARS-CoV-2. *Nanomedicine: Nanotechnology, Biology and Medicine*, Vol. 34, 2021, id. 102372.
[116] Al-Halifa, S., L. Gauthier, D. Arpin, S. Bourgault, and D. Archambault. Nanoparticle-based vaccines against respiratory viruses. *Frontiers in Immunology*, Vol. 10, 2019, id. 22.
[117] Farooq, M. U., V. Novosad, E. A. Rozhkova, H. Wali, A. Ali, A. A. Fateh, et al. Gold nanoparticles-enabled efficient dual delivery of anticancer therapeutics to HeLa cells. *Scientific Reports*, Vol. 8, No. 1, 2018, id. 2907.
[118] You, J., J. Zhou, M. Zhou, Y. Liu, J. Robertson, D. Liang, et al. Pharmacokinetics, clearance, and biosafety of polyethylene glycol-coated hollow gold nanospheres. *Particle and Fibre Toxicology*, Vol. 11, No. 1, 2014, id. 26.
[119] Movia, D., V. Gerard, C. M. Maguire, N. Jain, A. P. Bell, V. Nicolosi, et al. A safe-by-design approach to the development of gold nanoboxes as carriers for internalization into cancer cells. *Biomaterials*, Vol. 35, No. 9, 2014, pp. 2543–2557.
[120] Khan, H. A., M. A. K. Abdelhalim, M. S. Al-Ayed, and A. S. Alhomida. Effect of gold nanoparticles on glutathione and malondialdehyde levels in liver, lung and heart of rats. *Saudi Journal of Biological Sciences*, Vol. 19, No. 4, 2012, pp. 461–464.
[121] Uchiyama, M. K., D. K. Deda, S. F. De Paula Rodrigues, C. C. Drewes, S. M. Bolonheis, P. K. Kiyohara, et al. *In vivo* and *in vitro* toxicity and anti-inflammatory properties of gold nanoparticle bioconjugates to the vascular system. *Toxicological Sciences*, Vol. 142, No. 2, 2014, pp. 497–507.
[122] Ferchichi, S., H. Trabelsi, I. Azzouz, A. Hanini, A. Rejeb, O. Tebourbi, et al. Evaluation of oxidative response and tissular damage in rat lungs exposed to silica-coated gold nanoparticles under static magnetic fields. *International Journal of Nanomedicine*, Vol. 11, 2016, pp. 2711–2719.
[123] Adewale, O. B., H. Davids, L. Cairncross, and S. Roux. Toxicological Behavior of Gold Nanoparticles on Various Models: Influence of Physicochemical Properties and Other Factors. *International Journal of Toxicology*, Vol. 38, No. 5, 2019, pp. 357–384.
[124] Bashandy, M. M., A. R. Ahmed, M. El-Gaffary, and S. S. A. El-Rahman. Gold nanoparticle: synthesis, characterization, clinico-pathological, pathological, and bio-distribution studies in rabbits. In: *Pharmacological and Pharmaceutical Sciences International Scholarly and Scientific Research & Innovation*, International Journal of Innovation and Scientific Research, UK, 2015.
[125] Glazer, E. S., C. Zhu, A. N. Hamir, A. Borne, C. S. Thompson, and S. A. Curley. Biodistribution and acute toxicity of naked gold nanoparticles in a rabbit hepatic tumor model. *Nanotoxicology*, Vol. 5, No. 4, 2011, pp. 459–468.
[126] Sharma, A., A. Tandon, J. C. K. Tovey, R. Gupta, J. D. Robertson, J. A. Fortune, et al. Polyethylenimine-conjugated gold nanoparticles: Gene transfer potential and low toxicity in the cornea. *Nanomedicine*, Vol. 7, No. 4, 2011, pp. 505–513.
[127] De Berardis, B., M. Marchetti, A. Risuglia, F. Ietto, C. Fanizza, and F. Superti. Exposure to airborne gold nanoparticles: a review of current toxicological data on the respiratory tract. *Journal of Nanoparticle Research*, Vol. 22, 2020, id. 235.
[128] Leonavičiene, L., G. Kirdaite, R. Bradunaite, D. Vaitkiene, A. Vasiliauskas, D. Zabulyte, et al. Effect of gold nanoparticles in the treatment of established collagen arthritis in rats. *Medicina (Lithuania)*, Vol. 48, No. 2, 2012, pp. 91–101.
[129] Lignère, G. C., S. Giavarini, and S. Longatti. Initial experience with oral gold salts in the treatment of rheumatoid arthritis in patients followed up for one year. *Journal of International Medical Research*, Vol. 12, No. 3, 1984, pp. 193–197.
[130] Goldberg, R. L. *A mechanism of action of gold in rheumatoid arthritis. A biochemical and morphological investigation of the direct effect of gold sodium thiomalate (GST) on human synovial cells in cultuRE*. Open Access Dissertations, University of Rhode Island, [Kingston, RI], 1980.
[131] Freyberg, R. H., W. D. Block, and S. Levey. Metabolism, toxicity and manner of action of gold compounds used in the treatment of arthritis. I. human plasma and synovial fluid concentration and urinary excretion of gold during and following treatment with gold sodium thiomalate, gold sodium thiosul. *Journal of Clinical Investigation*, Vol. 20, No. 4, 1941, pp. 401–412.
[132] James, W. D., L. R. Hirsch, J. L. West, P. D. O'Neal, and J. D. Payne. Application of INAA to the build-up and clearance of gold nanoshells in clinical studies in mice. *Journal of Radioanalytical and Nuclear Chemistry*, Vol. 271, No. 2, 2007, pp. 455–459.
[133] Fernández de Castro, I., L. Sanz-Sánchez, and C. Risco. Metallothioneins for correlative light and electron microscopy, *Methods Cell Biol*. Vol. 124, 2014, pp. 55–70.
[134] Lansdown, A. B. G.. Gold: human exposure and update on toxic risks. *Critical Reviews in Toxicology*, Vol. 48, No. 7, 2018, pp. 596–614.
[135] Kusiak, R. A., J. Springer, A. C. Ritchie, and J. Muller. Carcinoma of the lung in Ontario gold miners: possible aetiological factors. *Occupational and Environmental Medicine*, Vol. 48, No. 12, 1991, pp. 808–817.
[136] Eisler, R.. Mercury hazards from gold mining to humans, plants, and animals. *Reviews of Environmental Contamination and Toxicology*, Vol. 181, 2005, pp. 139–198.

[137] Lansdown, A. B. G.. Chapter 13. Precious metals: silver, gold and platinum-related metals. In: *The Carcinogenicity of Metals: Human Risk Through Occupational and Environmental Exposure*, International Journal of Toxicology, 2013, pp. 278–300.

[138] Zhang, X. D., D. Wu, X. Shen, P. X. Liu, Y. M. Sun, L. A. Zhang et al. Size-dependent *in vivo* toxicity of PEG-coated gold nanoparticles. *International Journal of Nanomedicine*, Vol. 6, 2011, id. 2071.

[139] De Jong, W. H., W. I. Hagens, P. Krystek, M. C. Burger, A. J. A. M. Sips, and R. E. Geertsma. Particle size-dependent organ distribution of gold nanoparticles after intravenous administration. *Biomaterials*, Vol. 2912, 2008, pp. 1912–1919.

[140] Connor, E. E., J. Mwamuka, A. Gole, C. J. Murphy, and M. D. Wyatt. Gold nanoparticles are taken up by human cells but do not cause acute cytotoxicity. *Small*, Vol. 1, No. 3, 2005, pp. 325–327.

[141] Cho, W. S., S. Kim, B. S. Han, W. C. Son, and J. Jeong. Comparison of gene expression profiles in mice liver following intravenous injection of 4 and 100nm-sized PEG-coated gold nanoparticles. *Toxicology Letters*, Vol. 191, No. 1, 2009, pp. 96–102.

[142] Chithrani, B. D., A. A. Ghazani, and W. C. W. Chan. Determining the size and shape dependence of gold nanoparticle uptake into mammalian cells. *Nano Letters*, Vol. 6, No. 4, 2006, pp. 662–668.

[143] Van Doren, E. A. F., P. J. R. H. De Temmerman, M. A. D. Francisco, and J. Mast. Determination of the volume-specific surface area by using transmission electron tomography for characterization and definition of nanomaterials. *Journal of Nanobiotechnology*, Vol. 9, No. 1, 2011, id. 17.

[144] Fanord, F., K. Fairbairn, H. Kim, A. Garces, V. Bhethanabotla, and V. K. Gupta. Bisphosphonate-modified gold nanoparticles: a useful vehicle to study the treatment of osteonecrosis of the femoral head. *Nanotechnology*, Vol. 22, No. 3, 2011, id. 35102.

[145] Yokoyama, K. and A. Ichiki. Spectroscopic investigation on the affinity of SARS-CoV-2 spike protein to gold nano-particles. *Colloids and Interface Science Communications*, Vol. 40, 2021, id. 100356.

[146] Moitra, P., M. Alafeef, K. Dighe, M. B. Frieman, and D. Pan. Selective naked-eye detection of SARS-CoV-2 mediated by N gene targeted antisense oligonucleotide capped plasmonic nanoparticles. *ACS Nano*, Vol. 14, No. 6, 2020, pp. 7617–7627.

[147] Chang, S. Y., K. Y. Huang, T. L. Chao, H. C. Kao, Y. H. Pang, L. Lu, et al. Nanoparticle composite TPNT1 is effective against SARS-CoV-2 and influenza viruses. *Scientific Reports*, Vol. 11, No. 1, 2021, id. 8692.

[148] Babaei, A., S. M. Mousavi, M. Ghasemi, N. Pirbonyeh, M. Soleimani, and A. Moattari. Gold nanoparticles show potential *in vitro* antiviral and anticancer activity. *Life Sciences*, Vol. 284, 2021, id. 119652.

[149] Kim, J., M. Yeom, T. Lee, H. O. Kim, W. Na, A. Kang, et al. Porous gold nanoparticles for attenuating infectivity of influenza A virus. *Journal of Nanobiotechnology*, Vol. 18, No. 1, 2020, id. 54.

[150] Gopinath, S. C. B., K. Awazu, M. Fujimaki, K. Shimizu, and T. Shima. Observations of immuno-gold conjugates on influenza viruses using waveguide-mode sensors. *PLoS ONE*, Vol. 8, No. 7, 2013, id. e69121.

[151] Chen, L., H. Wei, Y. Guo, Z. Cui, Z. Zhang, and X. E. Zhang. Gold nanoparticle enhanced immuno-PCR for ultrasensitive detection of Hantaan virus nucleocapsid protein. *Journal of Immunological Methods*, Vol. 346, No. 1–2, 2009, pp. 64–70.

[152] Dong, H., J. Liu, H. Zhu, C. Y. Ou, W. Xing, M. Qiu, et al. Two types of nanoparticle-based bio-barcode amplification assays to detect HIV-1 p24 antigen. *Virol J*, Vol. 9, No. 2012, 2012, id. 180.

[153] El-Husseini, D. M., N. M. Helmy, and R. H. Tammam. The effect of gold nanoparticles on the diagnostic polymerase chain reaction technique for equine herpes virus 1 (EHV-1). *RSC Advances*, Vol. 660, 2016, pp. 54898–54903.

[154] Huang, S. H., T. C. Yang, M. H. Tsai, I. S. Tsai, H. C. Lu, P. H. Chuang, et al. Gold nanoparticle-based RT-PCR and real-time quantitative RT-PCR assays for detection of Japanese encephalitis virus. *Nanotechnology*, Vol. 1940, 2008, id. 405101.

[155] Perez, J. W., E. A. Vargis, P. K. Russ, F. R. Haselton, and D. W. Wright. Detection of respiratory syncytial virus using nanoparticle amplified immuno-polymerase chain reaction. *Analytical Biochemistry*, Vol. 410, No. 1, 2011, pp. 141–148.

[156] Alafeef, M., K. Dighe, P. Moitra, and D. Pan. Rapid, Ultrasensitive, and quantitative detection of SARS-CoV-2 using antisense oligonucleotides directed electrochemical biosensor chip. *ACS Nano*, Vol. 14, No. 12, 2020, pp. 17028–17045.

[157] Mahari, S., A. Roberts, D. Shahdeo, and S. Gandhi. eCovSens-ultrasensitive novel in-house built printed circuit board based electrochemical device for rapid detection of nCovid-19 antigen, a spike protein domain 1 of SARS-CoV-2. *BioRxiv*, 2020.

[158] Layqah, L. A. and S. Eissa. An electrochemical immunosensor for the corona virus associated with the Middle East respiratory syndrome using an array of gold nanoparticle-modified carbon electrodes. *Microchimica Acta*, Vol. 186, No. 4, 2019, id. 224.

[159] Okoye, N. C., A. P. Barker, K. Curtis, R. R. Orlandi, E. A. Snavely, C. Wright, et al. Performance characteristics of binaxnoW COVID-19 antigen card for screening asymptomatic individuals in a university setting. *Journal of Clinical Microbiology*, Vol. 59, No. 4, 2021.

[160] Schuler, C. F., C. Gherasim, K. O'Shea, D. M. Manthei, J. Chen, D. Giacherio, et al. Accurate point-of-care serology tests for COVID-19. *PLoS ONE*, Vol. 16, No. 3, March, 2021, id. e0248729.

[161] Krüger, L. J., J. A. F. Klein, F. Tobian, M. Gaeddert, F. Lainati, S. Klemm, et al. Evaluation of accuracy, exclusivity, limit-of-detection and ease-of-use of LumiraDx™: An antigen-detecting point-of-care device for SARS-CoV-2. *Infection*, Vol. 50, No. 2, 2022, pp. 395–406.

[162] Brihn, A., J. Chang, K. OYong, S. Balter, D. Terashita, Z. Rubin, et al. Diagnostic Performance of an Antigen Test with RT-PCR for the Detection of SARS-CoV-2 in a Hospital Setting – Los Angeles County, California, June–August 2020. *MMWR Recommendations and Reports*, Vol. 70, No. 19, 2021, pp. 702–706.

[163] Li, T., L. Wang, H. Wang, X. Li, S. Zhang, Y. Xu, et al. Serum SARS-COV-2 Nucleocapsid Protein: A Sensitivity and Specificity Early Diagnostic Marker for SARS-COV-2 Infection. *Frontiers in Cellular and Infection Microbiology*, Vol. 10, 2020, id. 00470.

[164] FDA. Sienna TM-Clarity COVIBLOCK TM COVID-19 lgG/lgM Rapid Test Cassette (Whole Blood/Plasma/Serum/Fingerstick Whole Blood). 2020.

[165] Tuaillon, E., K. Bolloré, A. Pisoni, S. Debiesse, C. Renault, S. Marie, et al. Detection of SARS-CoV-2 antibodies using commercial assays and seroconversion patterns in hospitalized patients. *Journal of Infection*, Vol. 81, No. 2, 2020, pp. e39–e45.

[166] Ravi, N., D. L. Cortade, E. Ng, and S. X. Wang. Diagnostics for SARS-CoV-2 detection: A comprehensive review of the FDA-EUA COVID-19 testing landscape. *Biosensors and Bioelectronics*, Vol. 165, 2020, id. 112454.

[167] Hsiao, W. W. W., T. N. Le, D. M. Pham, H. H. Ko, H. C. Chang, C. C. Lee, et al. Recent advances in novel lateral flow technologies for detection of COVID-19. *Biosensors*, Vol. 11, No. 9, 2021, id. 295.

[168] Lin, Y. C., C. Y. Cheng, C. P. Chen, S. H. Cheng, S. Y. Chang, and P. R. Hsueh. A case of transient existence of SARS-CoV-2 RNA in the respiratory tract with the absence of anti-SARS-CoV-2 antibody

response. *International Journal of Infectious Diseases*, Vol. 96, 2020, pp. 464–466.
[169] Valera, E., A. Jankelow, J. Lim, V. Kindratenko, A. Ganguli, K. White, et al. *COVID-19 Point-of-Care Diagnostics: Present and Future*, 15, ACS NaAmerican Chemical Society, 2021, pp. 7899–7906.
[170] Zainol Rashid, Z., S. N. Othman, M. N. Abdul Samat, U. K. Ali, and K. K. Wong. Diagnostic performance of COVID-19 serology assays. *The Malaysian Journal of Pathology*, Vol. 42, No. 1, 2020, pp. 13–21.
[171] Cho, W. S., M. Cho, J. Jeong, M. Choi, H. Y. Cho, B. S. Han, et al. Acute toxicity and pharmacokinetics of 13 nm-sized PEG-coated gold nanoparticles. *Toxicology and Applied Pharmacology*, Vol. 236, No. 1, 2009, pp. 16–24.
[172] Hwang, J. H., S. J. Kim, Y. H. Kim, J. R. Noh, G. T. Gang, B. H. Chung, et al. Susceptibility to gold nanoparticle-induced hepatotoxicity is enhanced in a mouse model of nonalcoholic steatohepatitis. *Toxicology*, Vol. 294, No. 1, 2012, pp. 27–35.
[173] Chen, J., H. Wang, W. Long, X. Shen, D. Wu, S. S. Song, et al. Sex differences in the toxicity of polyethylene glycol-coated gold nanoparticles in mice. *International Journal of Nanomedicine*, Vol. 8, 2013, id. 2409.
[174] Yang, C., A. Tian, and Z. Li. Reversible cardiac hypertrophy induced by PEG-coated gold nanoparticles in mice. *Scientific Reports*, Vol. 6, No. 1, 2016, id. 20203.
[175] Chen, Y. S., Y. C. Hung, I. Liau, and G. S. Huang. Assessment of the *in vivo* toxicity of gold nanoparticles. *Nanoscale Res Lett*, Vol. 4, No. 8, 2009, pp. 858–864.
[176] Ziaee Ghahnavieh, M., M. Ajdary, M. Ziaee Ghahnavieh, and N. Naghsh. Effects of intraperitoneal injection of gold nanoparticles in male mice. *Nanomedicine Journal*, Vol. 1, No. 2, 2014, pp. 121–127.
[177] Zhang, X., H. ying Wu, D. Wu, Y. Wang, J. Chang, Z. bin Zhai, et al. Toxicologic effects of gold nanoparticles *in vivo* by different administration routes. *International Journal of Nanomedicine*, Vol. 5, 2010, id. 771.
[178] Chen, H., A. Dorrigan, S. Saad, D. J. Hare, M. B. Cortie, and S. M. Valenzuela. *In vivo* study of spherical gold nanoparticles: inflammatory effects and distribution in mice. *PLoS ONE*, Vol. 8, No. 2, 2013, id. e58208.
[179] Lasagna-Reeves, C., D. Gonzalez-Romero, M. A. Barria, I. Olmedo, A. Clos, V. M. Sadagopa Ramanujam, et al. Bioaccumulation and toxicity of gold nanoparticles after repeated administration in mice. *Biochemical and Biophysical Research Communications*, Vol. 393, No. 4, 2010, pp. 649–655.
[180] Sun, P. P., C. S. Lai, C. J. Hung, P. Dhaiveegan, M. L. Tsai, C. L. Chiu, et al. Subchronic oral toxicity evaluation of gold nanoparticles in male and female mice. *Heliyon*, Vol. 7, No. 3, 2021, id. e06577.
[181] Sengupta, J., P. Datta, H. K. Patra, A. K. Dasgupta, and A. Gomes. *In vivo* interaction of gold nanoparticles after acute and chronic exposures in experimental animal models. *Journal of Nanoscience and Nanotechnology*, Vol. 13, No. 3, 2013, pp. 1660–1670.
[182] Tomuleasa, C., C. Berce, C. Lucan, B. Petrushev, S. Boca, M. Miclean, et al. *In vivo* assessment of bone marrow toxicity by gold nanoparticle-based bioconjugates in Crl:CD1(ICR) mice. *International Journal of Nanomedicine*, Vol. 11, 2016, pp. 4261–4273.
[183] Venkatpurwar, V., V. Mali, S. Bodhankar, and V. Pokharkar. *In vitro* cytotoxicity and *in vivo* sub-acute oral toxicity assessment of porphyran reduced gold nanoparticles. *Toxicological & Environmental Chemistry*, Vol. 94, No. 7, 2012, pp. 1357–1367.
[184] Abdelhalim, M. and B. M. Jarrar. Histological alterations in the liver of rats induced by different gold nanoparticle sizes, doses and exposure duration. *Journal of Nanobiotechnology*, Vol. 10, No. 1, 2012, id. 5.
[185] Siddiqi, N. J., M. A. K. Abdelhalim, A. K. El-Ansary, A. S. Alhomida, and W. Y. Ong. Identification of potential biomarkers of gold nanoparticle toxicity in rat brains. *Journal of Neuroinflammation*, Vol. 9, No. 1, 2012, id. 656.
[186] Doudi, M. and M. Setorki. The effect of gold nanoparticle on renal function in rats. *Nanomedicine J*, Vol. 1, No. 3, 2014, pp. 171–179.
[187] Khan, H. A., M. A. K. Abdelhalim, A. S. Alhomida, and M. S. Al-Ayed. effects of naked gold nanoparticles on proinflammatory cytokines mRNA expression in rat liver and kidney. *BioMed Research International*, Vol. 2013, 2013, pp. 1–6.
[188] Rambanapasi, C., J. Zeevaart, H. Buntting, C. Bester, D. Kotze, R. Hayeshi, et al. Bioaccumulation and Subchronic Toxicity of 14 nm Gold Nanoparticles in Rats. *Molecules*, Vol. 21, No. 6, 2016, id. 763.
[189] Rathore, M., I. R. Mohanty, U. Maheswari, N. Dayal, R. Suman, and D. S. Joshi. Comparative *in vivo* assessment of the subacute toxicity of gold and silver nanoparticles. *Journal of Nanoparticle Research*, Vol. 16, No. 4, 2014, id. 2338.
[190] Muller, A. P., G. K. Ferreira, S. da Silva, R. T. Nesi, G. de Bem Silveira, C. Mendes, et al. Safety protocol for the gold nanoparticles administration in rats. *Materials Science and Engineering: C*, Vol. 77, 2017, pp. 1145–1150.
[191] Jo, M. R., S. H. Bae, M. R. Go, H. J. Kim, Y. G. Hwang, and S. J. Choi. Toxicity and Biokinetics of Colloidal Gold Nanoparticles. *Nanomaterials*, Vol. 5, No. 2, 2015, pp. 835–850.
[192] Fraga, S., A. Brandão, M. E. Soares, T. Morais, J. A. Duarte, L. Pereira, et al. Short- and long-term distribution and toxicity of gold nanoparticles in the rat after a single-dose intravenous administration. *Nanomedicine: Nanotechnology, Biology and Medicine*, Vol. 10, No. 8, 2014, pp. 1757–1766.
[193] Patibandla, S., Y. Zhang, A. M. Tohari, P. Gu, J. Reilly, Y. Chen, et al. Comparative analysis of the toxicity of gold nanoparticles in zebrafish. *Journal of Applied Toxicology*, Vol. 38, No. 8, 2018, pp. 1153–1161.
[194] Truong, L., S. C. Tilton, T. Zaikova, E. Richman, K. M. Waters, J. E. Hutchison, et al. Surface functionalities of gold nanoparticles impact embryonic gene expression responses. *Nanotoxicology*, Vol. 7, No. 2, 2013, pp. 192–201.
[195] Kim, K. T., T. Zaikova, J. E. Hutchison, and R. L. Tanguay. Gold nanoparticles disrupt zebrafish eye development and pigmentation. *Toxicological Sciences*, Vol. 133, No. 2, 2013, pp. 275–288.
[196] Sangabathuni, S., R. V. Murthy, P. M. Chaudhary, B. Subramani, S. Toraskar, and R. Kikkeri. Mapping the glyco-gold nanoparticles of different shapes toxicity, biodistribution and sequestration in adult zebrafish. *Scientific Reports*, Vol. 7, No. 1, 2017, id. 4239.
[197] Dedeh, A., A. Ciutat, M. Treguer-Delapierre, and J. P. Bourdineaud. Impact of gold nanoparticles on zebrafish exposed to a spiked sediment. *Nanotoxicology*, Vol. 9, No. 1, 2015, pp. 71–80.
[198] Hassanen, E. I., E. A. Morsy, A. M. Hussien, M. A. Ibrahim, and K. Y. Farroh. The effect of different concentrations of gold nanoparticles on growth performance, toxicopathological and immunological parameters of broiler chickens. *Bioscience Reports*, Vol. 40, No. 3, 2020.
[199] Vecchio, G., A. Galeone, V. Brunetti, G. Maiorano, S. Sabella, R. Cingolani, et al. Concentration-dependent, size-independent toxicity of citrate capped AuNPs in *Drosophila melanogaster*. *PLoS ONE*, Vol. 7, No. 1, 2012, id. e29980.